

AD-A084 750

AMERICAN ELECTRONIC LABS INC LANSDALE PA
SPATIAL PULSE COMPRESSION.(U)
MAR 80 P STEINBACH

F/8 9/5

UNCLASSIFIED

RADC-TR-80-43

F30602-77-C-0136
NL

1 of 1
AD-A
064 150

END
DATE
FILMED
9-80
DTIC

ADA 084750

RADC-TR-80-43
Final Technical Report
March 1980

(12)
SC

LEVEL II



SPATIAL PULSE COMPRESSION

American Electronics Laboratories, Inc.

Philip Steinbach

APPROVED FOR PUBLIC RELEASE; DISTRIBUTION UNLIMITED

Laboratory Directors' Fund No. 01707708

DTIC
ELECTE
MAY 28 1980
S D A

ROME AIR DEVELOPMENT CENTER
Air Force Systems Command
Griffiss Air Force Base, New York 13441

DDC FILE COPY

80 5 27 210

This report has been reviewed by the RADC Public Affairs Office (PA) and is releasable to the National Technical Information Service (NTIS). At NTIS it will be releasable to the general public, including foreign nations.

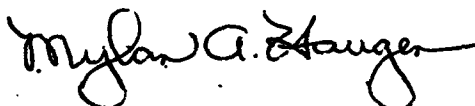
RADC-TR-80-43 has been reviewed and is approved for publication.

APPROVED:




PAUL VAN ETTEN
Project Engineer

APPROVED:



MYLAN A. HAUGEN, Lt Col, USAF
Chief, Surveillance Division

FOR THE COMMANDER:



JOHN P. HUSS
Acting Chief, Plans Office

This effort was funded totally by the Laboratory Directors' Fund.

If your address has changed or if you wish to be removed from the RADC mailing list, or if the addressee is no longer employed by your organization, please notify RADC (OCTS), Griffiss AFB NY 13441. This will assist us in maintaining a current mailing list.

Do not return this copy. Retain or destroy.

UNCLASSIFIED

SECURITY CLASSIFICATION OF THIS PAGE (When Data Entered)

19 REPORT DOCUMENTATION PAGE		READ INSTRUCTIONS BEFORE COMPLETING FORM	
1. REPORT NUMBER RADG-TR-80-431	2. GOVT ACCESSION NO. ADA084750	3. RECIPIENT'S CATALOG NUMBER	
4. TITLE (and Subtitle) SPATIAL PULSE COMPRESSION		5. TYPE OF REPORT & PERIOD COVERED Final Technical Report Jul 1977 - Oct 1979	
7. AUTHOR(s) Philip Steinbach		8. CONTRACT OR GRANT NUMBER(s) F30602-77-C-0136	
9. PERFORMING ORGANIZATION NAME AND ADDRESS American Electronics Laboratories, Inc. P.O. Box 552 Lansdale PA 19446		10. PROGRAM ELEMENT, PROJECT, TASK AREA & WORK UNIT NUMBERS 61101F 01707708	
11. CONTROLLING OFFICE NAME AND ADDRESS Rome Air Development Center (OCTS) Griffiss AFB NY 13441		12. REPORT DATE March 1980	
14. MONITORING AGENCY NAME & ADDRESS (if different from Controlling Office) Same		13. NUMBER OF PAGES 87	
		15. SECURITY CLASS. (of this report) UNCLASSIFIED	
		15a. DECLASSIFICATION/DOWNGRADING SCHEDULE N/A	
16. DISTRIBUTION STATEMENT (of this Report) Approved for public release; distribution unlimited.			
17. DISTRIBUTION STATEMENT (of the abstract entered in Block 20, if different from Report) Same			
18. SUPPLEMENTARY NOTES RADG Project Engineer: Paul Van Etten (OCTS) This effort was funded under the RADG Laboratory Directors Fund 01707708.			
19. KEY WORDS (Continue on reverse side if necessary and identify by block number) Broadband antenna electromagnetic fields antenna dispersion pulse compression			
20. ABSTRACT (Continue on reverse side if necessary and identify by block number) The purpose of this experiment is to verify that the characteristics of a broadband antenna will cause it to function as a dispersive filter. A log-periodic type antenna with a bandpass from 50 MHz to 1000 MHz is used. To determine the proper waveform, a transmitting antenna was driven with a 2 nanosecond impulse and the resulting waveform which was a chirp			

DD FORM 1 JAN 73 1473

EDITION OF 1 NOV 65 IS OBSOLETE

UNCLASSIFIED

(Cont'd)

SECURITY CLASSIFICATION OF THIS PAGE (When Data Entered)

402008

DM

UNCLASSIFIED

SECURITY CLASSIFICATION OF THIS PAGE(When Data Entered)

Item 20 (Cont'd)

pulse, was measured at a receiving antenna.

A generator was constructed to produce the time-inverse of the measured waveform, which was driven into the transmitting antenna. The signal at the output of the receiver antenna was measured and observed to be an impulse with processing gain.

The antenna range was calibrated using a CW signal of the same amplitude as the transmitted signal. The processing gain of the system is defined as the ratio of the impulse amplitude and was measured at approximately 20 dB. For this system, the theoretical gain is approximately 23 dB.

The generator was a passive device consisting of an array of 46 calibrated coaxial delay lines which delay the front of a step-input waveform. The resulting delayed signals are added, in time, in a series of power combiners to provide the up-chirp pulse.

UNCLASSIFIED

SECURITY CLASSIFICATION OF THIS PAGE(When Data Entered)

EVALUATION

American Electronic Laboratories was successful in building and demonstrating a chirp waveform generator. This generator was employed to a set of dispersive antennas in which spatial pulse compression was demonstrated. The successes in this program have added to the Air Force's goal of obtaining large energy content in a wideband impulsive waveform.

Paul Van Elteren

PAUL VAN ETTEN
Project Engineer

Account Number _____
Name _____
Room No. _____
Telephone No. _____
Classification _____

Distribution / _____

Availability Codes _____

List	Available and/or Special
A	

TABLE OF CONTENTS

Part		Page
	Introduction	7
I	Determination Of The Logarithmic Chirp Waveform That Matches The Combined Impulse Response Of Two AEL APN-995B Coplanar Log-Periodic Antennas	13
II	Experimental Results Of Radiation Field Compression By The Conjugate Despersive Impulse Response Of Two AEL APN-955B Coplanar Log-Periodic Antennas	29
	Conclusions	61
Appendix 1	Theory Of The Reconciliation Of Several Slightly Differing Empirical Graphs Of A Single, Underlying Logarithmic Downchirp Waveform	1-1
Appendix 2	Waveform Graphs Recently Obtained, Showing Portions Of The Combined Impulse Response Of Two AEL Coplanar Log-Periodic Antennas, Type APN-995B	2-1
Appendix 3	Relevant Computer Printout Sheets (Done Via HP 9825A Desk-Top Calculator)	3-1
Appendix 4	Computer Modeling Of A Log-Periodic Antenna	4-1

LIST OF ILLUSTRATIONS

Figure		Page
1	View of Emitter Constructed by AEL	8
2	View of Emitter Constructed by AEL	9
3	AEL Model APN-995B Coplanar Log Periodic Antenna	10

LIST OF TABLES

Table		Page
1	Results Of Analyzing Each Of Five Waveform-Graphs For Logarithmic Periodicity Of Zero-Crossings	17
2	Behavior Of The Error-Measures E and U Near Their Minima, Versus The Parameter K	22
3	Comparison Of Down-Chirp - Waveform Parameters From The Recent AEL Tests, And For The Much Earlier RADC Tests, On The Impulse Response Of Paired APN-995B Antennas	25

INTRODUCTION

This report presents the findings and results of experimental testing conducted by AEL to determine chirp waveform response that matched the combined impulse response of two AEL Model APN-995B Coplanar Log-Periodic Antennas. This testing was performed in accordance with the requirements of the contractual documents related to Contract F30602-77-C-0136. These results, along with a comprehensive investigation into the associated design criteria and the related field compressive and dispersive response technology, will be detailed in this report.

In order to conduct these tests to the stipulated RADC requisites, AEL designed, developed, and constructed an emitter that would fulfill the radiation and power density requirements of this program. This emitter was constructed to meet the imposed stringent standards and procedures. The emitter is shown in Figures 1 and 2. As required, for this intensive electromagnetic field testing, two AEL Model APN-995B Coplanar Log-Periodic Antennas were employed with the AEL-built exciter as a pulse compression network for this contract. See Figure 3 for a photograph of the antenna.

Radiated emissions were obtained, measured, and recorded with the resulting hard copy of the tests presented herein together with its associated technical data.

In addition to the experimental testing, analysis was also conducted by AEL on the resulting data to reconcile differences in empirical graphs of a single, underlying logarithmic down chirp waveform. These results are presented in Appendix 1. Appendix 2 presents the actual graphs obtained during the testing of two AEL Model APN-995B Coplanar Log-Periodic Antennas. Appendix 3 presents the detailed results of AEL's analysis, highlighting the resulting zero-crossing times of the desired up-chirp waveform. Appendix 4 is a reprint of an article detailing "Computer Modeling of a Log Periodic Antenna". Conclusions are presented at the end of the body of this report.

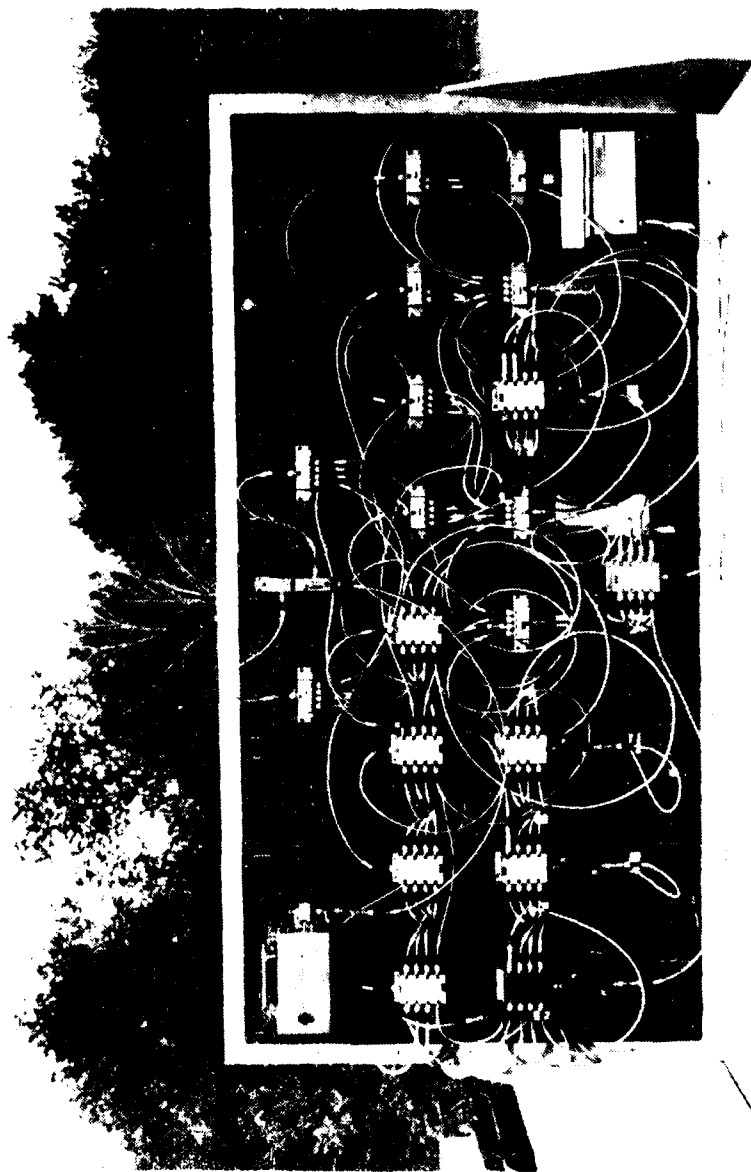


Figure 1. View of Emitter Constructed by AEL

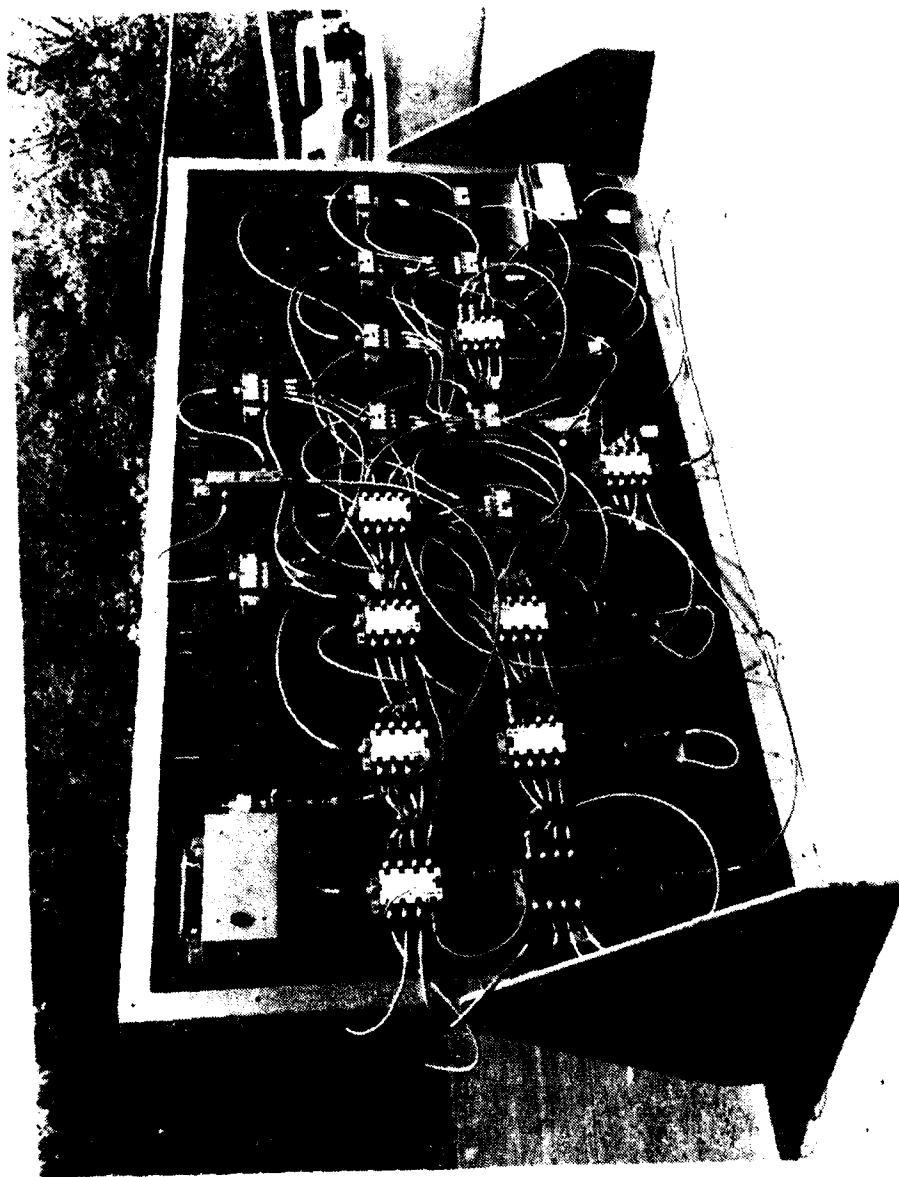


Figure 2. View of Emitter Constructed by AEL

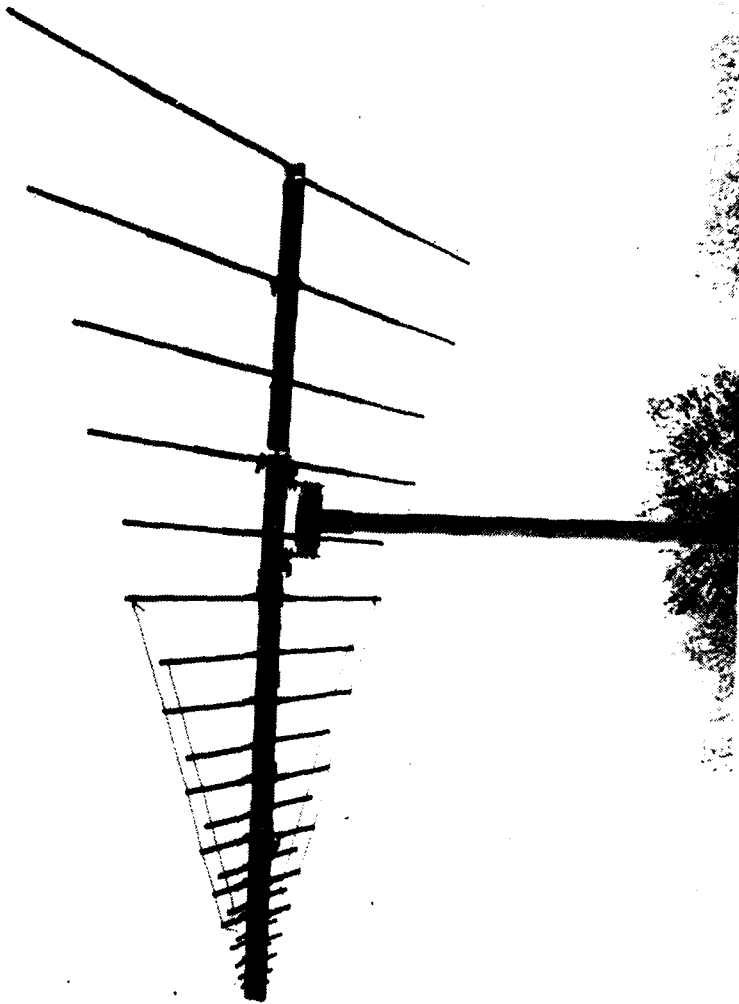


Figure 3. AEL Model APN-995B Coplanar Log Periodic Antenna

PART I

**DETERMINATION OF THE LOGARITHMIC CHIRP
WAVEFORM THAT MATCHES THE COMBINED
IMPULSE RESPONSE OF TWO AEL APN-995B
COPLANAR LOG-PERIODIC ANTENNAS**

PART I

DETERMINATION OF THE LOGARITHMIC CHIRP WAVEFORM THAT MATCHES THE COMBINED IMPULSE RESPONSE OF TWO AEL APN-995B COPLANAR LOG-PERIODIC ANTENNAS

Two of the APN-995B antennas were set up on a pattern range, facing each other nose-to-nose, one was excited by a fractional-nanosecond pulse, and the down-chirping output of the other was presented to a sampling oscilloscope, whose output was conveniently obtained in hard copy through the use of a chart recorder instead of a camera.

Several waveform graphs were thus obtained, showing portions of the combined impulse response of the two antennas, plus the cable that was involved (insofar as that impulse response is approximated by the down-chirp waveform actually observed). Five of these waveform graphs were selected for data reduction, with attention centering primarily on the timing of the zero-crossings of the oscillatory waveform involved. The uneven pattern of relative amplitudes of the successive positive and negative peaks of the waveform, although not of primary interest for this immediate investigation, was instrumental in permitting the different zero-crossings shown in the various waveform graphs to be identified unambiguously, independently of the graph upon which they appeared, and thus to be assigned a single, coherent ordinal numbering, consistent from one graph to the next. Copies of the five graphs are shown in Appendix 2.

The five graphs selected for analysis were as follows:

"GRAPH 2": Shows substantially all of the impulse-response or, down-chirp, waveform (at least 180 nSec of it), but at a relatively slow sweep rate of 20 nSec/inch. Zero-crossings from the eighth to the fifty-first were clearly measurable; those prior to the eighth were identifiable, but were not very well measurable because of overlapping of their ink traces; those subsequent to the forty-seventh were not of interest, through corresponding to instantaneous frequencies too far below 50 MHz. The eighth through the forty-seventh zero-crossings were carefully measured as to time of occurrence (in a manner which is described farther below), and corresponded to a range of instantaneous frequencies from about 750 MHz down to 47 MHz.

"GRAPH 4": Shows the beginning of the down-chirp waveform, at a greatly expanded sweep rate of 2 nSec/inch, enabling clear identification of its zero-crossings down to the "0th" (at its tangible start), and permitting accurate measurement of the times of occurrence of the zero-crossings from the first up to and including the sixteenth, covering the range from 1.24 GHz down to 430 MHz. This graph controls the ordinal numbering of all the zero-crossings.

"GRAPH 5": Shows the first three-quarters of the down-chirp waveform, at an intermediate sweep rate of 10 nSec/inch, permitting clear identification and accurate measurements of zero-crossings from the 0th to the thirty-seventh, which cover the range from 1.33 GHz down to 96 MHz.

"GRAPH 6": Shows the latter half of the main part of the down-chirp waveform, but not its very end, and again at a sweep rate of 10 nSec/inch. Zero-crossings from the twenty-eighth to the forty-sixth are clear and measurable, and cover the range from approximately 180 MHz down to 51 MHz.

"GRAPH 7": Shows the end of the down-chirp waveform region of interest, with zero-crossings from the thirty-ninth to the fifty-first clearly identifiable and measurable. However, only those up to and including the forty-seventh were measured, covering the range from approximately 84 MHz down to 47 MHz. It was fortuitous that the portion of the waveform past the forty-seventh zero-crossing was not of interest, because degradation of the wave-shape to a nonsinusoidal shape occurred there.

The 48 zero-crossings of interest (of ordinal numbers 0 through 47), on the five graphs previously described, were measured as to time of occurrence with the aid of a binocular microscope equipped with a reticle marked in 0.001 inch divisions: The reticle scale was used to estimate the center of the (0.024 inch to 0.026 inch wide) ink trace produced by the chart recorder. The locations of the zero-crossings on the chart-recorder graphs were obtained with a precision of a few thousandths of an inch, hence of picoseconds to tens of picoseconds in time, depending upon the sweep rate of the graph; this precision, although it far exceeds the absolute accuracy that can be claimed for the same zero-crossing times, is useful because it all but eliminates

the observation of the graphs themselves as a source of error in determining the properties of the underlying chirp waveform that they separately and collectively portray. On each graph, for convenience, the left-hand margin of the graph was initially taken as an arbitrary time-reference origin.

As the first step in the analysis of the zero-crossing time data from the five graphs measured, the zero-crossing data for each graph, separately, were fitted by the theoretical log-down-chirp formula:

$$N = A \ln T - B, \quad (1)$$

where N ideally represents the ordinal number of the zero-crossing, if an integer, but represents a noninteger number of half-cycles otherwise; A and B are undetermined constant coefficients; and, T represents the empirically determined time t of the zero-crossing, shifted by an amount D which is the same for all the zero-crossings on the same graph, i. e.,

$$T = t + D. \quad (2)$$

The method of fitting the data was as follows. A given time-origin shift D was provisionally assumed, and was used to shift each observed zero-crossing time to a new value T , according to Equation (2). The resulting collection of T -data for the graph being analyzed was then fitted maximally well by the formula (1), by choosing the constant coefficients A and B according to the method of least squares: the quantity that was minimized was the sum of the squares of the discrepancies between the right-hand side of Equation (1) and the ordinal number N of the zero-crossing in question, evaluated over all the zero-crossings on the graph. This minimized sum-of-squares of (essentially) phase-discrepancies-at-zero-crossings was then calculated, and tabulated versus different values assigned to the time-shift D , to empirically find the best value of D , that gave the smallest value for the A -and- B -minimized sum of squares of zero-crossing phase discrepancies. In this way, an optimized set of values was determined for the entire set of three coefficients A , B , and D , completely fixing the theoretical equation that best represented the zero-crossing data for the graph. The accompanying computer printout sheets (Appendix 3) labeled C1 through C5 show the

final results of this phase of the analysis, obtained separately for each of the five waveform graphs of interest; these sheets are self-explanatory. The computer used was a desk-top programmable calculator, Hewlett-Packard 9825A. All of its printouts are shown in Appendix 3.

The essential results of the printouts (C1 to C5) are summarized in the following table, in which the coefficients C and K belong to the formula,

$$T = C K^N, \quad (3)$$

which is the inverse of Equation (1), and which gives the theoretical T-scale time of occurrence of a zero-crossing if the ordinal number N of the zero-crossing is specified.

For purposes of comparison, a sixth row of entries, for a graph no. "0", has been added to Table 1 to show the results of a reanalysis of the data concerning the times of positive peaks of the down-chirp waveform that was shown in RADC Oscillogram Photo RADC-OC-74-79. The results of this reanalysis, done by the present more mathematically sophisticated method, are traced in greater detail on the computer printout sheet C6; these results slightly correct and update the earlier analysis of the RADC-OC-74-79 Oscillogram Photo that was presented in Technical Appendix A of AEL Proposal No. 18538-4373. (Note that the "K" value of 1.1484, that was derived in the earlier analysis of that Oscillogram Photo, was a log-change factor per full cycle, so that its square root, or, 1.0716, is a K-factor per half-cycle, which can be directly compared to the newer values that are listed here for parameter K.)

Because of the fact that the ordinal number N is essentially a position coordinate that counts half-cycles of the chirp waveform, N is conveniently assigned integer values at the zero-crossings of the chirp waveform (as in printouts C1 through C5); but it must then, instead, be assigned values that differ by one-half unit from integers when peaks of the chirp waveform are being described (as in printout C6). The choice of the particular ordinal-number position "N = -5.5 half-cycles", for the first datum listed in printout C6, (e. g., as opposed to N = 6.5 or N = -4.5, etc.), serves to put the ordinal numbering of the measured waveform peaks on Oscillogram Photo RADC-OC-74-79 into maximally good agreement (as far as can be determined) with the

TABLE 1
RESULTS OF ANALYZING EACH OF FIVE WAVEFORM-GRAPHS FOR LOGARITHMIC
PERIODICITY OF ZERO-CROSSINGS

Graph	Best Value of Shift of Time-Origin (nSec for Equation 2)	Best Values of Parameters for Theoretical Zero-Crossing Formulas (for Equation 1) (for Equation 3)				Minimized Residual Error of Equation (1) (in Cycles of Oscillation)	Implied Length of Pulse to Cover 50 MHz to 1.05 GHz	
		<u>A</u>	<u>B</u>	<u>C</u>	<u>K</u>		Half-Cycles	Duration in nSec
2	-19.4	14.042	23.102	5.1817	<u>1.0738</u>	0.0337	42.8	133.7
4	-2.54	14.525	25.211	5.6728	<u>1.0713</u>	0.0176	44.2	138.3
5	-22.7	14.042	23.491	5.3277	<u>1.0738</u>	0.0291	42.8	133.7
6	+36.5	13.879	22.181	4.9441	<u>1.0747</u>	0.0201	42.3	132.2
7	+70.0	12.650	15.128	3.3065	<u>1.0823</u>	0.0188	38.5	120.5

"0" (see text, pp. 17 and 18)	+0.5	13.936	23.406	5.3635	<u>1.0744</u>	0.0559	42.4	132.7

mutually consistent ordinal numberings assigned to the zero-crossings of the five new waveform graphs that have here been reported via printouts C1 through C5. Particularly, the ordinal numbering N adopted on printout C6 puts that sheet's resulting value of the parameter C into maximally good agreement with the value of C that comes out of the mathematical reconciliation of the five new waveform graphs (i.e., Graphs 2, 4, 5, 6, and 7) which is described next. It should be noted that the different possible ordinal numberings, that might have been used on printout C6 in place of the one actually used there, differ only by what is essentially a coordinate shift, in N, and, therefore, would only affect the values of the parameters C and B, and not the value of the log-change factor K, nor the value of the related parameter A.

The numerical results entered in the parameter columns A, B, C, and K in Table 1 show quite good agreement between the graphs 2, 4, 5, and 6, with some departure occurring in Graph 7; and these output data agree remarkably well with those for "Graph 0", representing the waveform RADC-OC-74-79, which was taken several years earlier and with a different pair of the APN-995B antennas. Particularly, in Table 1, the consistency of the different K-values is most impressive, which is important, because K is the principal chirp waveform parameter: K, as used here, is the factor by which the half-period of the down-chirp increases during each successive half-cycle of its oscillation.

The mutual consistency of the parameter values, displayed in Table 1 for the five graphs of current interest, is sufficiently good that a final set of parameter values might have been assigned by arbitrarily averaging the parameters of the five separate graphs. But a more sophisticated reconciliation of the data from the different graphs was deemed desirable, that would in essence subject all of their data simultaneously to a single least-squares reduction; and that would also allow for, and from a statistical standpoint shed some light on, slight uncertainties in the relative sweep rates of the different waveform graphs. Accordingly, a complete theoretical method was devised for performing such an over-all analysis and reconciliation of the data; this method is developed in full mathematical detail in the accompanying Appendix 1.

With reference to equation locations numbered in Appendix 1, the numerical analysis of the data proceeds as follows. (Optional portions of the discussion, which

discuss calculations that do not need to be performed for present purposes, but which may be helpful in illustrating the logic of the theoretical method employed, are indented for clarity.) The zero-crossing times t_{NM} specified in (7) are measured, and constitute the totality of input data for the analysis. A trial value for the parameter K is then assumed outright, somewhere in the general vicinity of 1.07 (see Table 1). The five different sums which can be identified as contributing to the right-hand sides of (21) and (22) are next calculated, and from them the quantities Q_M and R_M are calculated via (21) and (22), for each of the waveform graphs (which are distinguished via the subscript M); the values of some of the contributing sums are retained for later use in certain other formulas.

The five calculated values R_M , together with the known numbers of data points, J_M , defined at (16.5), can in principle be used to compute the best value of the parameter C (for the assumed K) from the formula (28) which involves two further sums; and this value of C , together with the quantities Q_M and R_M already calculated, can in principle be used to calculate best time-scale adjustment factors S_M , and best time-origin shift amounts D_M , for the various graphs, via (20) and (19) respectively, which in essence optimize the fit of the empirical zero-crossings by a single theoretical log-chirp waveform; the scale-adjustment factors S_M , and the time-shifts D_M , are usable as in (8), to adjust the raw empirical zero-crossing times t_{NM} to produce optimally reduced empirical zero-crossing times, T_{NM} , which are suitable to be compared, as in (10), with theoretical logarithmic-down-chirp zero-crossing times computable from the formula (9).

But the process that can be visualized as starting from formula (28) — of computing the individual time-discrepancies between the reduced-empirical and the theoretical zero-crossings, of re-expressing each discrepancy as a phase discrepancy referred to the local period of the chirp, and of computing the (minimized) RMS value "E" of all of these phase discrepancies of zero-crossings, for all of the five waveform graphs taken together — is all conveniently bypassed, simply by using the formula

(31) which is based upon quantities that are already known, and which gives the desired E directly, not even requiring the knowledge of the value of the parameter C . In a similar way, the criterion that leads to the best value for C (i.e., that the scale-adjustment factors S_M should in a collective sense depart minimally from their ideal value of unity) also gives the convenient formula (33) for a quantity U that expresses how large that minimal departure must be: U of (33) represents the minimum possible fractional (convertible to percent) amount by which the time-scale adjustment factors S_M for the five graphs must be assumed to depart from the ideal value unity (collectively, in weighted RMS value of their individual deviations from unity) in order to maximize the closeness of fit of all of the zero-crossings by a single mathematical log-chirp formula. Thus, merely by proceeding through the formulas (21), (22), (31) with definitions (16.5) and (27), and (33), the quantities E and U are calculated, which are respectively, the best RMS phase-fit to zero-crossings, and the smallest weighted-RMS readjustment of time-scales that is needed — best, and smallest, that is, for the assumed value of K , which, however, may not itself be an optimum value! Therefore, the entire process of calculating best- E and smallest- U values is to be repeated for a selection of different assumed values of K , to find, by trial-and-error, a best value for K , which would simultaneously minimize both E and U . Although this procedure would be difficult for hand calculation, it runs easily on the programmable desk-top calculator, and quickly localizes the best range for K . As is sketched in (34) in Appendix 1, the error-measures E and U are not actually minimized simultaneously for a single value of K ; but their separate minima versus K define a very narrow range for K , enabling a best, compromise value of K to be selected, which carries considerable certainty, as will be further described in the ensuing discussion of numerical results.

The process previously described, of calculating a least error E of phase-fit of zero-crossings, and a least measure U of time-scale readjustments that are needed to optimize the fit, versus values arbitrarily assumed for the parameter K , gives the numerical results shown in Table 2 when that process is applied to the empirical zero-crossing data, which is comprised of the entries appearing in the first two columns (t versus N) of the accompanying computer printout sheets C1 to C5.

From Table 2, it is seen that the best value of K is bracketed tightly between the values 1.0721 and 1.0738, which minimize U and E , respectively: this is the "range of compromise" which was illustrated in a qualitative way in the sketch (34) in Appendix 1. In this range of K , broadened to round the end values of K to the nearest 0.0005 unit, the values of U that are encountered do not exceed 1.82 percent, and thus represent putative time-scale errors that are easily supportable in view of the time-accuracy of the experimental apparatus — sufficiently easily justifiable, in fact, that a strict minimization of the error-measure U loses importance compared to the minimization of the phase-error measure E . On this basis, the value of K that minimizes E ($K = 1.0738$) could be chosen to be the final value for K ; but inspection of Table 2 shows that a small movement, to slightly smaller values of K , makes a worthwhile reduction in the value of U , while only inappreciably increasing the value of E . Particularly, in going from $K = 1.0738$ to 1.0735, U decreases by about 16% of itself, while E increases in value by only 2.3 percent of itself. Although the further motion, of lowering K to 1.0730, would decrease U by somewhat more than 20 percent further, it would do so in a range of U where U is already small compared to possible experimental time-scale errors; and such further motion would increase E by an additional 12 percent of its minimum value, marking an undesirable upward acceleration of the value of E . Through these considerations, and to a precision of 0.0005 unit in K (which represents a moderately good precision of 0.7 percent in the determination of the quantity " $K-1$ "), the analysis that has been traced suggests that the final value for K be taken to be:

$$K = \underline{1.0735} \text{ (dimensionless).} \quad (4)$$

For this best value of K , the formula (28) in Appendix 1 yields the following best value for the remaining parameter, C , that is needed to completely specify the theoretical logarithmic down-chirp formula, Equation (3):

$$C = \underline{5.3036} \text{ (nanoseconds).} \quad (5)$$

The statistical analysis developed in Appendix 1 gives not only a best value for the parameter C once K is chosen, but also gives best values for the factors by which the

TABLE 2
BEHAVIOR OF THE ERROR-MEASURES E AND U NEAR THEIR MINIMA,
VERSUS THE PARAMETER K

K	E	U
Assumed Value of the Log-Change Factor per Half-Cycle (ratio)	Minimized RMS Value of Zero-Crossing Phase-Discrepancies (degrees)	Minimized Required (Weighted-RMS) Time-Scale Readjustment (percent)
1.0700	28.79	2.05
1.0705	25.49	1.62
1.0710	22.27	1.21
1.0715	19.19	0.85
1.0720	16.29	0.63
<u>1.072135</u> -----	<u>15.56</u> -----	<u>0.6184</u>
1.0725	13.71	0.70
1.0730	11.64	1.01
1.0735	10.38	1.39
<u>1.073810</u> -----	<u>10.1507</u> -----	1.65
1.0740	10.24	1.82
1.0745	11.24	2.25
1.0750	13.11	2.70
1.0755	15.55	3.15
1.0760	18.32	3.60
1.0765	21.29	4.05
1.0770	24.37	4.50
1.0775	27.54	4.96
1.0780	30.76	5.41

time-scales of all of the experimental waveform graphs should be assumed to be in need of alteration to produce a best fit of the empirical zero-crossings by the theoretical log-chirp formula. These and other numerical results of the analysis in Appendix 1, for the value (4) of K , are displayed on the accompanying computer printout sheet C7, which is quite well self-explanatory. On sheet C7, just below the main table of entries, there are listed the optimal time-shifts and the optimal time-scale readjustment factors for each of the five experimentally obtained waveform graphs. None of the five time-scale readjustment factors implies a time-scale correction larger than 2 percent; and the five time-scale factors have a weighted RMS value of only 1.4% (Column U in Table 2). The five time-shifts that are listed on sheet C7 are figured as being applied before the time-scale factors are applied to the waveform graphs, and therefore do not correspond exactly to the quantities D_M of the analysis in Appendix 1, but instead to the quantities D_M/S_M there (see Equation (8) of Appendix 1, and its text).

The second column, T, on sheet C7, lists the theoretical log-down-chirp zero-crossings, computed from Equation (3) with the optimum K and C from (4) and (5). The five main columns on sheet C7 then list the discrepancies in time between these theoretical values and the (reduced — via Equation 8 of Appendix 1) empirically observed zero-crossings. All of these discrepancies are less than 1 nanosecond, and just over half of them (and practically all of the ones for early zero-crossings, $N < 16$) are less, and in many instances, much less, than 0.1 nanosecond. As listed on sheet C7, these various time discrepancies, when converted to discrepancies of oscillation phase at each measured zero crossing, have an RMS value of only 10.4 degrees of phase — for 122 separate measurements made on the 48 zero-crossings of interest. This result implies a rather impressive degree of agreement between the observed zero-crossings and those of an ideal, mathematical, logarithmic-down-chirp waveform, and justifies considerable confidence in the values derived above for the waveform parameters K and C , stated in (4) and (5).

The very close agreement, that is found between the present measurements and those which are in effect retrospectively made by the reanalysis of the earlier waveform photo RADC-OC-74-79, is noteworthy; this agreement is of considerable interest

from the standpoint of reproducibility of chirp waveforms by physical structures, because physically distinct pairs of the AEL APN-995B coplanar log-periodic antennas were involved in the much earlier tests at RADC, than in the present tests at AEL: One of the antennas that was used in the recent tests was manufactured at least 40 months later, and the other approximately 56 months later, than the two antennas that had been tested at RADC. Table 3 makes a point-by-point comparison of the final calculated results, on the one hand, for the reanalysis of the RADC-OC-74-79 waveform photo, and, on the other hand, for the statistical reconciliation of the five waveform graphs of interest from the recent AEL tests (these two sets of data are taken from the computer printout sheets C6 and C7, respectively, which have been discussed previously).

Again, as in Table 1, the agreement of K-values is impressive. The final measurement result, that the chirp's frequency region of primary interest spans about 43 half-cycles of oscillation, jibes excellently well with earlier expectations, and fits quite satisfactorily into the range of capability of the inverse chirp generator under construction, which is designed to be able to output as many as 47 half-cycles of oscillation if desired.

Out of scientific curiosity, an initial effort has been made, outside the present project, to try to understand the latest and best value for K in terms of some geometrical ratio that is characteristic of the mechanical structure of the APN-995B antennas. This separate effort has so far turned up the following interesting and simple comparison: Whereas the down-chirp waveform's period has now been empirically observed to grow by the factor 1.0735 per half-cycle, hence $(1.0735)^2$ or 1.1524 per full cycle, examination of the mechanical design specifications for the Type APN-995B antenna reveals that the ratios of the specified spacings between the successive arms of the antenna average 1.1550 (with a maximum individual deviation of about 1 percent of this figure) for the 25 different antenna arms that mount along each half of the central boom. The present note does not go further into these matters, or their theoretical discussion.

In synthesizing an up-chirp waveform that is to be a time-reversed replica of the observed logarithmic down-chirp waveform, it seems most practical to have the

TABLE 3
COMPARISON OF DOWN-CHIRP-WAVEFORM PARAMETERS FROM THE
RECENT AEL TESTS, AND FOR THE MUCH EARLIER RADC TESTS,
ON THE IMPULSE RESPONSE OF PAIRED APN-995B ANTENNAS

			Final Value from Least-Square Adjustment, for Best Fit of Empirical Data by an Ideal Logarithmic-Down-Chirp Waveform	
Quantity of Importance	Symbol	Units	Reanalysis of Earlier RADC Tests (see Sheet C6)	Analysis of Recent AEL Tests (see Sheet C7)
Period Growth-Factor per Half-Cycle	K	(ratio)	1.0744	1.0735
Time Scale Factor (see Equation (1) of Appendix 1)	C	nSec	5.3635	5.3036
Parameters for Half- Cycles Versus Time (see Equations(2) to (4) of Appendix 1)	A	half-cycles	13.936	14.100
	B	half-cycles	23.406	23.523
RMS Value of Dis- crepancies in Oscillation Phase at Fitted Points	E	degrees	20.14 (at peaks of one polarity)	10.38 (at zero- crossings)
Number of Fitted Points	---	---	22.	48.
Number of Individual Time-Measurements	---	---	22.	122.
Computed Location of "50 MHz"	N ₂	half-cycles	45.394	46.251
	T ₂	nSec	139.356	140.995
Computed Location of "1.05 GHz"	N ₁	half-cycles	2.967	3.325
	T ₁	nSec	6.636	6.714
Computed Width of Pulse Region of Interest	(N ₂ -N ₁)	half-cycles	42.427*	42.926
	(T ₂ -T ₁)	nSec	132.720*	134.281

*Previously analyzed as 44 half-cycles (essentially), and 139 nSec, respectively,
in Technical Appendix A of AEL Proposal 18538-4373.

synthesized pulse start and end at zero-crossings of the down-chirp waveform, even if the range of instantaneous frequencies that is thus covered goes slightly beyond the specified limits of 50 and 1050 MHz. Accordingly, with reference to the ideal pulse boundaries specified by the half-cycle locations N_2 and N_1 listed in the last column of Table 3, a practical up-chirp waveform should start at the forty-seventh zero-crossing of the down-chirp waveform and, counting backwards, end at the third zero-crossing of the down-chirp waveform, and should, thus, comprise a total of 45 zero-crossings (numbered conveniently from $N = 0$ to $N = 44$), with 44 intervening time-intervals. The range of instantaneous frequencies that this will cover (see the frequency formula that appears near the bottom of printout sheet C7, which is obtained by inverting formula (12) of Appendix 1) is, from about 47 to 1074 MHz, which encompasses the desired range of 50 to 1050 MHz. Accordingly, an ordinal number N has been assigned to zero-crossings of the desired up-chirp waveform by subtracting the ordinal number of the down-chirp's corresponding zero-crossing from the integer 47; this relationship is printed, for convenient reference, as the leading entry on the accompanying computer printout sheet C8 which summarizes the timing goals to be used for synthesis of the up-chirp pulse.

With the "(47-N)" reversal of ordinal numbering of zero-crossings, in going from the down-chirp to the up-chirp waveform, it would at first seem logical that the time coordinate of the up-chirp should be measured backwards from "148.685" nSec, the time of the down-chirp's forty-seventh zero-crossing (from the T-column of printout sheet C7). However, the considerations that follow indicate that it will instead be more meaningful and convenient to figure time for the up-chirp backwards from the forty-sixth zero-crossing of the down-chirp, at "138.505" nSec, thus giving the second formula that is printed at the top of printout sheet C8. First of all, the forty-sixth zero-crossing of the down-chirp (hence, the $N = 1$ zero-crossing of the up-chirp) corresponds to an instantaneous frequency of 50.9 MHz, and can, therefore, be labeled the "start" of the up-chirp without appreciably infringing upon the specified frequency range. Second, there is the consideration that the $N = 1$ zero-crossing of the synthesized up-chirp waveform will always be more cleanly defined in time than will the $N = 0$ zero-"crossing" of the up-chirp; for, at $N = 0$, where the synthesized

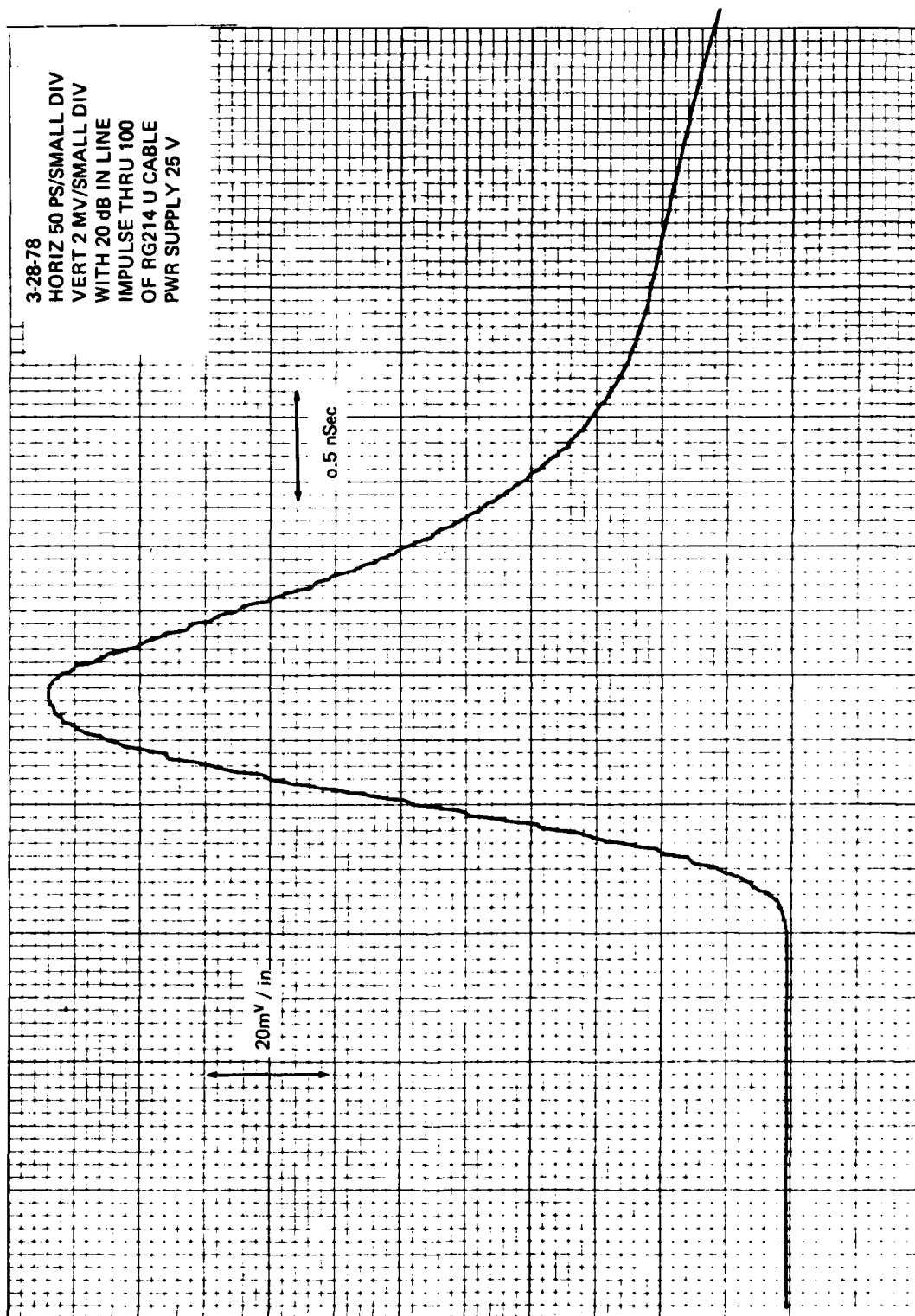
waveform will actually first depart from zero voltage, it will do so with a horizontal "toe", and not actually cross zero, whereas the $N = 1$ zero-crossing will consist of a clear reversal of polarity, cutting definitively through zero voltage. In other words, from a practical waveform standpoint, $N = 1$ will actually be the first clearly defined zero-crossing of the up-chirp waveform, and will thus constitute a more precise datum from which to measure time intervals associated with the up-chirp pulse. From this standpoint, the $N = 0$ location on the up-chirp pulse serves merely as a dummy zero-crossing which conveniently gets the up-chirp moving, and away from zero volts, so that the subsequent polarity reversals, which comprise the up-chirp's true zero-crossings of interest, can begin; the up-chirp's initial region, between $N = 0$ and $N = 1$, brackets instantaneous frequencies from 47.4 to 50.9 MHz whose accurate inclusion is not essential, and constitutes a single "dummy" half-cycle whose presence guarantees a more precise definition of the remainder of the up-chirp of interest, extending from $N = 1$ to $N = 44$.

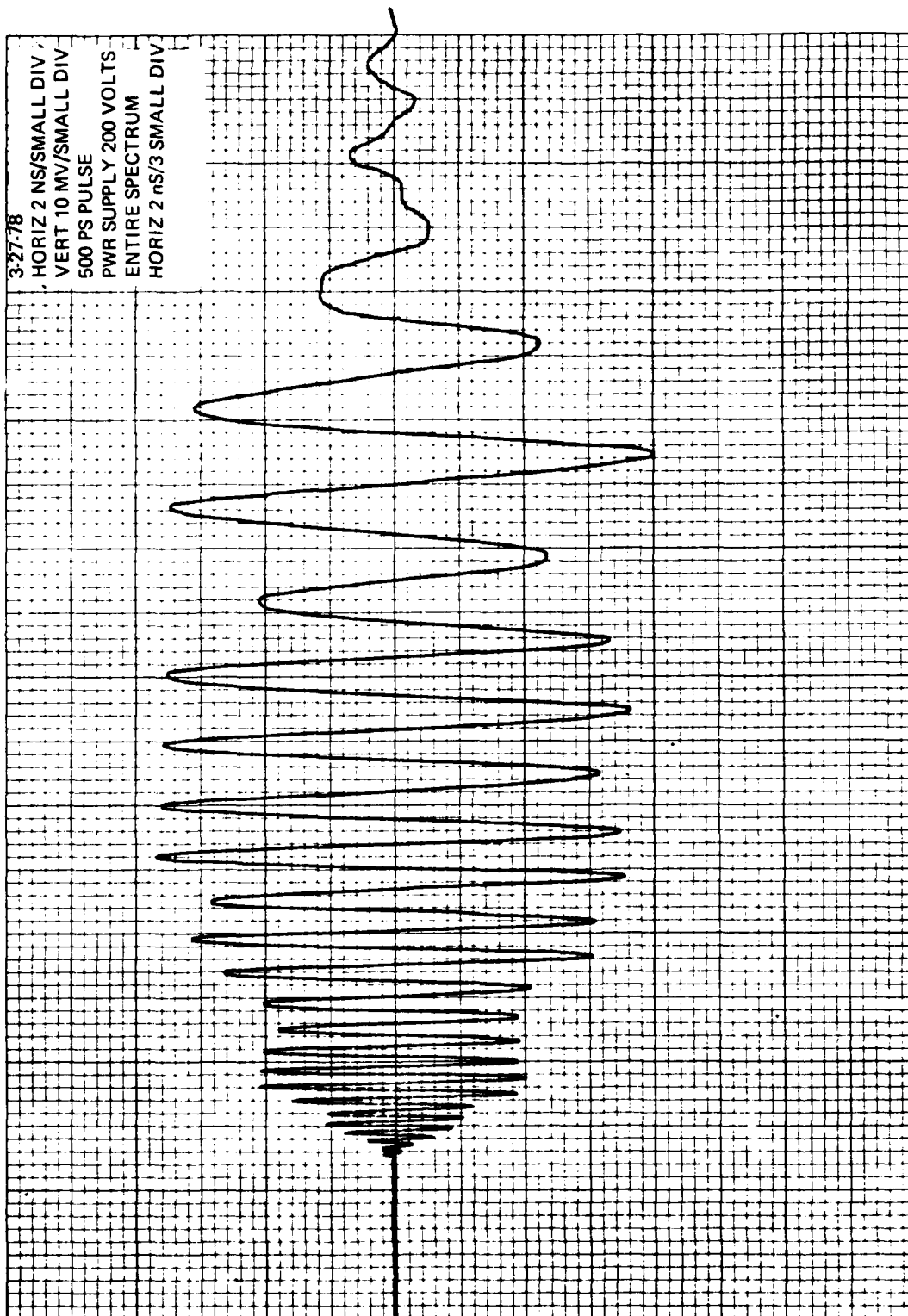
With the adoption of the "(47-N)" reversal of ordinal numbering, and of the "(138.505-T)" reversal of the time-coordinate measured in nanoseconds, both the ordinal numbering and the times of occurrence of the zero-crossings of the up-chirp waveform become well defined in terms of the corresponding entities of the down-chirp waveform, which are listed on printout sheet C7. The resulting complete plan of the time-reversing up-chirp pulse is tabulated for convenient reference in the main body of the accompanying computer printout sheet C8 (this tabulation is divided horizontally into blocks of 8 lines or 4 lines, which correspond to the main power divider/combiner units encountered by the output ends of the "500"-series of connecting cables in the pulse-synthesizing circuitry). Printout sheet C8 also displays formulas which are useful for interconverting any two of the three following quantities belonging to the planned up-chirp waveform: Elapsed time, T (measured from the $N = 1$ zero-crossing, as previously explained); elapsed number of half-cycles of oscillation, N (not necessarily an integer, in this context); and the instantaneous frequency, f . The derivation of the detailed plan for the up-chirp pulse, summarized on printout sheet C8, completes an important necessary step, and a logical phase, of the present program.

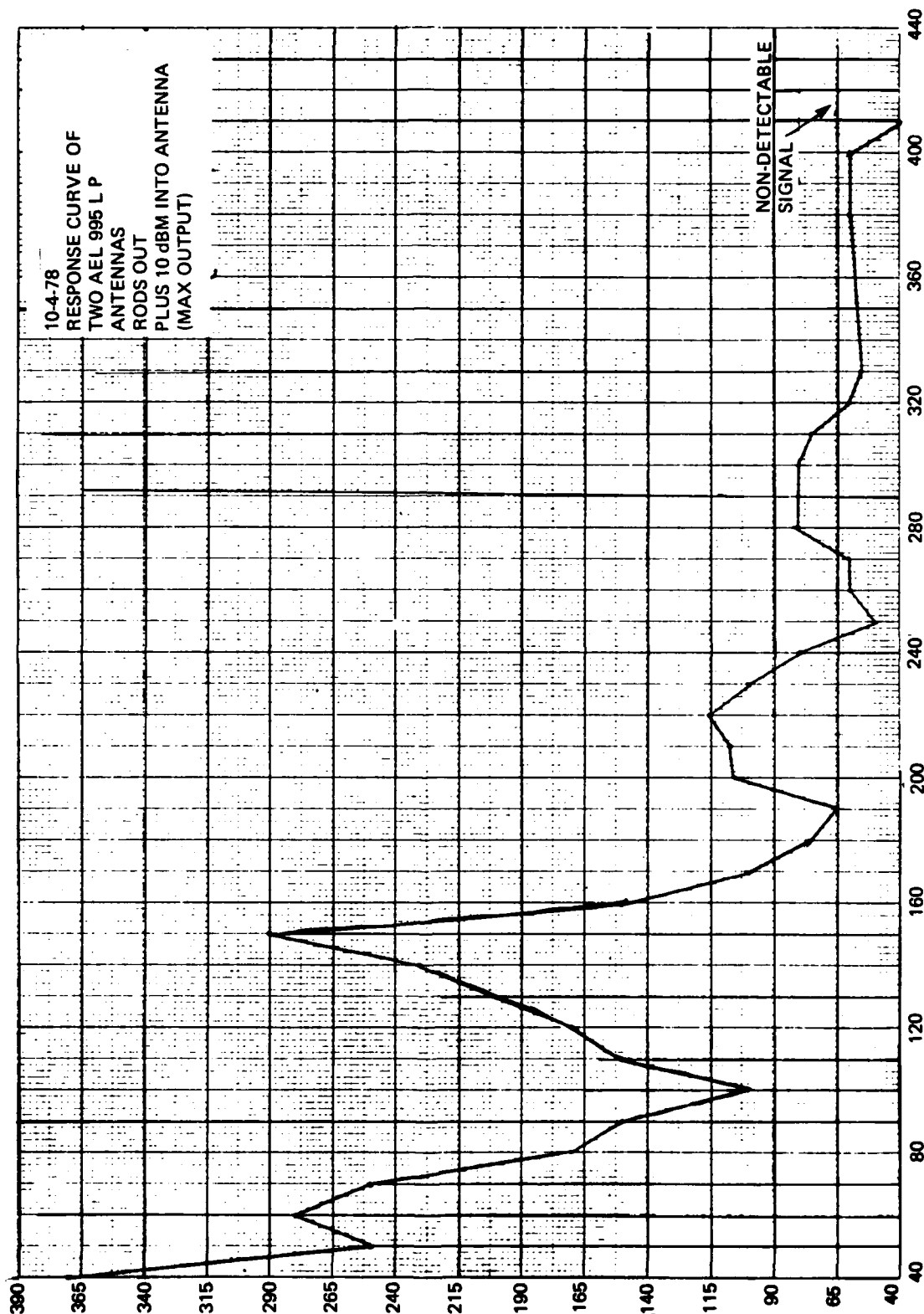
PART II

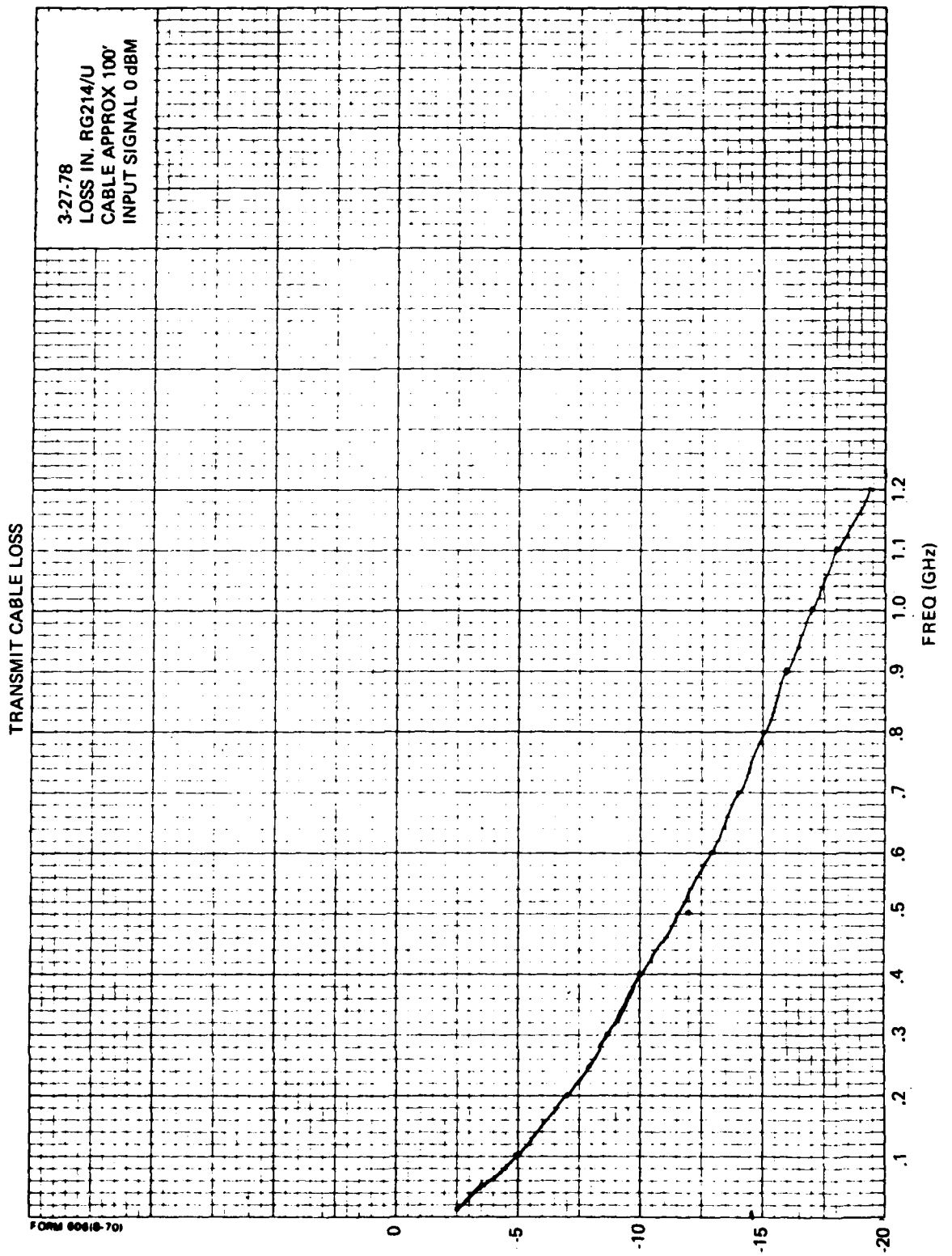
**EXPERIMENTAL RESULTS OF RADIATION FIELD
COMPRESSION BY THE CONJUGATE
DESPERSIVE IMPULSE RESPONSE OF TWO
AEL APN-955B COPLANAR
LOG-PERIODIC ANTENNAS**

3-28-78
HORIZ 50 PS/SMALL DIV
VERT 2 MV/SMALL DIV
WITH 20 dB IN LINE
IMPULSE THRU 100
OF RG214 U CABLE
PWR SUPPLY 25 V









**DATA ON THE CONJUGATE LOGARITHMIC UP-CHIRP
GENERATOR CONSTRUCTED AND TESTED
17 JANUARY 1979**

**DELAY CABLE DATA
MEASURED VERSUS CALCULATED**

Cable Number	Measured Zero Crossing (ns)	Calculated Zero Crossing (ns)	Time Difference		Group Time Difference (ns)
			Longer (ns)	Shorter (ns)	
500	10.15	10.180		0.03	0.97 Longer
501	9.3	9.483		0.183	
502	8.6	8.834		0.234	
503	8.5	8.229	0.271		
504	8.1	7.666	9.434		
505	7.6	7.140	0.46		
506	6.3	6.652		0.352	
507	<u>6.8</u>	<u>6.196</u>	<u>0.604</u>		
Total Time	65.35	64.38	1.769	0.799	
508	5.015	5.773		0.758	0.289 Shorter
509	5.75	5.377	0.373		
510	4.75	5.008		0.258	
511	4.75	4.666	0.084		
512	4.55	4.347	0.203		
513	3.95	4.048		0.098	
514	3.95	3.772	0.178		
515	<u>3.5</u>	<u>3.513</u>		<u>0.013</u>	
Total Time	36.215	36.504	0.838	1.127	
516	2.75	3.273		0.532	0.093 Longer
517	3.25	3.049	0.201		
518	2.35	2.840		0.49	
519	3.00	2.645	0.355		
520	2.70	2.465	0.235		
521	2.00	2.296		0.296	
522	2.50	2.138	0.362		
523	<u>2.25</u>	<u>1.992</u>	<u>0.258</u>		
Total Time	20.8	20.698	1.411	1.318	
524	1.76	1.856		0.096	0.256 Shorter
525	1.8	1.728			
526	1.50	1.611		0.111	
527	1.60	1.500	0.100		
528	1.30	1.397		0.097	
529	1.50	1.302	0.198		
530	.92	1.212		0.292	
531	<u>1.10</u>	<u>1.130</u>		<u>0.030</u>	
Total Time	11.48	11.736	0.370	0.626	

DELAY CABLE DATA
MEASURED VERSUS CALCULATED
(Continued)

Cable Number	Measured Zero Crossing (ns)	Calculated Zero Crossing (ns)	Time Difference		Group Time Difference (ns)
			Longer (ns)	Shorter (ns)	
532	0.98	1.052		0.072	0.136 Shorter
533	0.98	0.980	0.00	0.00	
534	0.80	0.913		0.113	
535	0.90	0.851	0.049		
Total Time	3.66	3.796	0.049	0.185	
536	0.78	0.792		0.012	0.322 Longer
537	0.78	0.738	0.042		
538	0.78	0.687	0.093		
539	0.84	0.641	0.199		
Total Time	3.18	2.858	0.334	0.012	
540	0.50	0.596		0.096	0.08 Longer
541	0.64	0.556	0.084		
542	0.61	0.518	0.092		
Total Time	1.75	1.67	0.176	0.096	

Remaining Cables, unable to measure.

CALCULATED TOTALS

64.38 ns
36.504 ns
20.698 ns
11.736 ns
3.796 ns
2.858 ns
1.67 ns
141.642 ns

MEASURED TOTALS

65.35 ns
36.215 ns
20.8 ns
11.48 ns
3.66 ns
3.18 ns
1.75 ns
142.435 ns

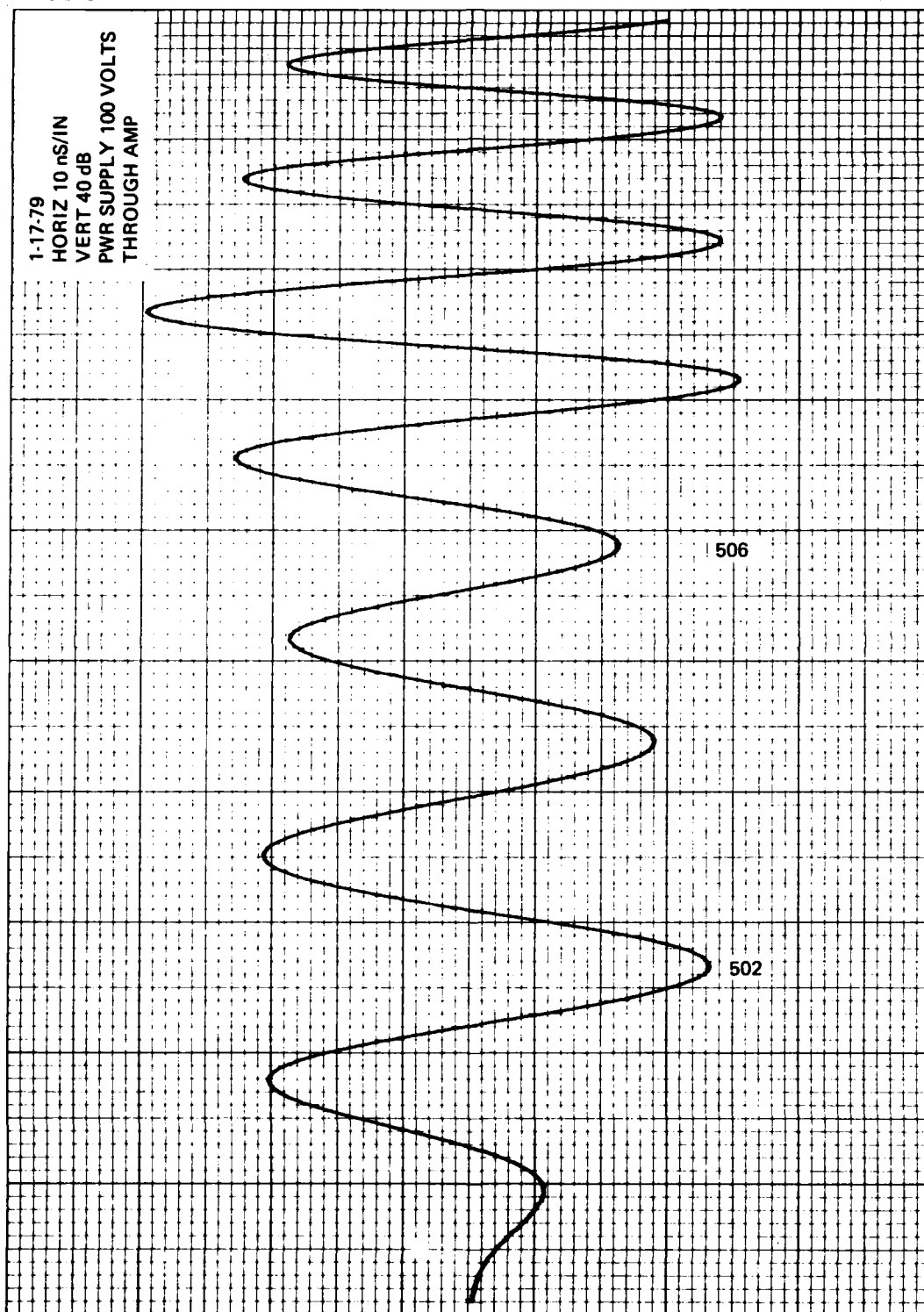
TOTAL MEASURED VALUES ARE 0.793 ns LONGER THAN CALCULATED VALUES.

80 MV (X 100)
8 VOLTS

0

80 MV (X 100)
8 VOLTS

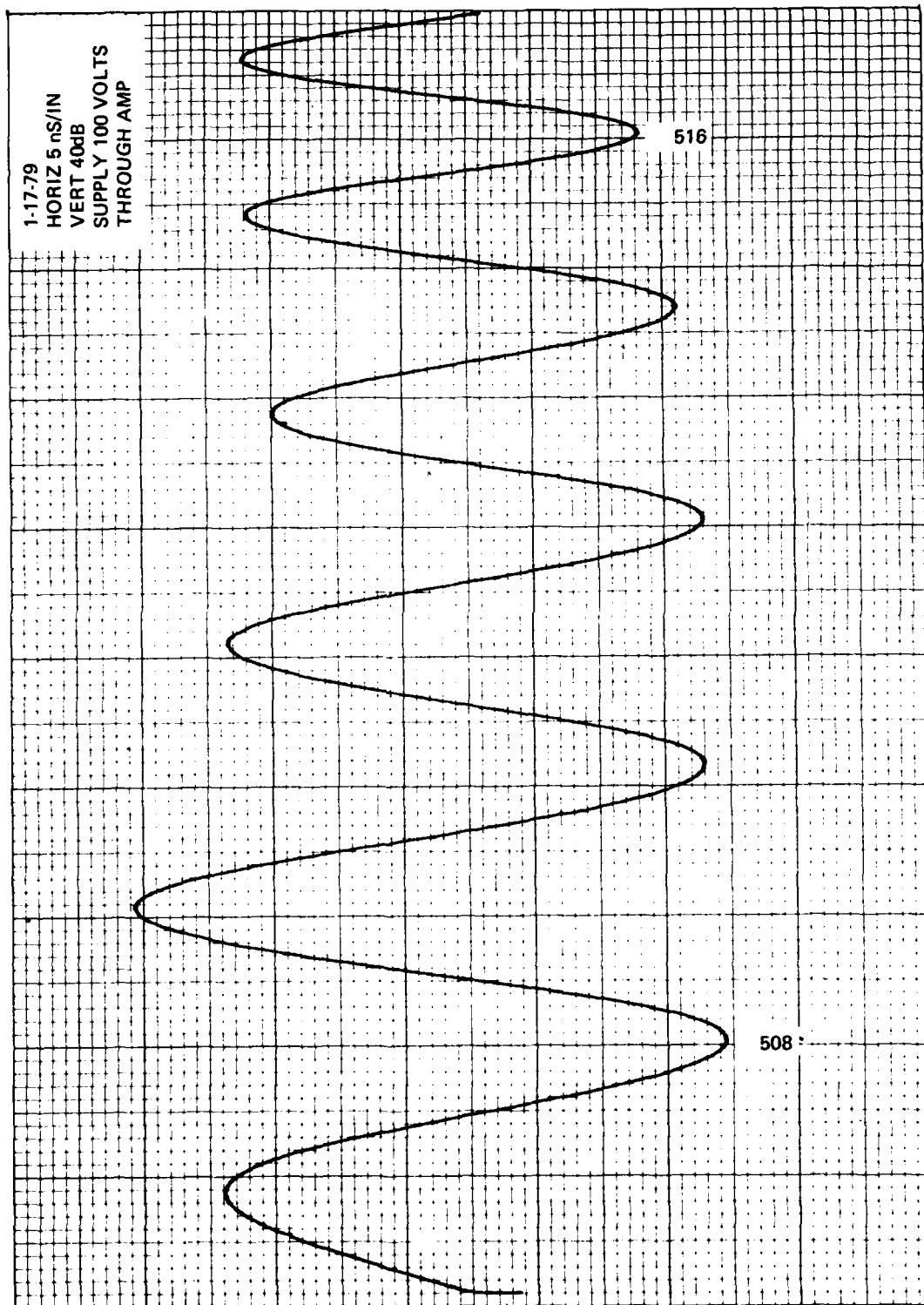
1-17-79
HORIZ 10 ns/IN
VERT 40 dB
PWR SUPPLY 100 VOLTS
THROUGH AMP



80 MV (X 100)
8 VOLTS

80 MV (X 100)
8 VOLTS

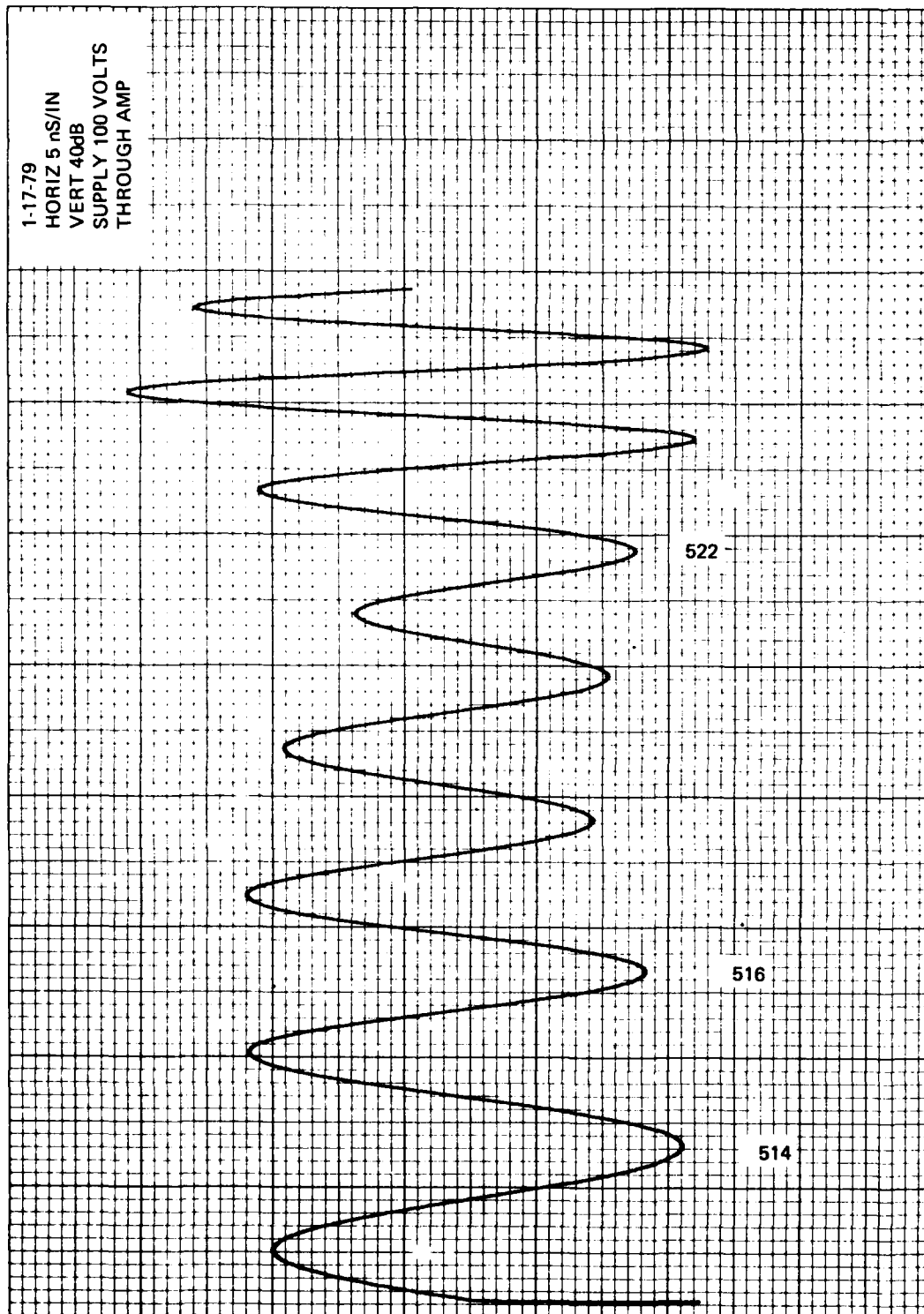
1-17-79
HORIZ 5 ns/IN
VERT 40dB
SUPPLY 100 VOLTS
THROUGH AMP



80 MV (X 100)
8 VOLTS

0

1-17-79
HORIZ 5 nS/IN
VERT 40dB
SUPPLY 100 VOLTS
THROUGH AMP

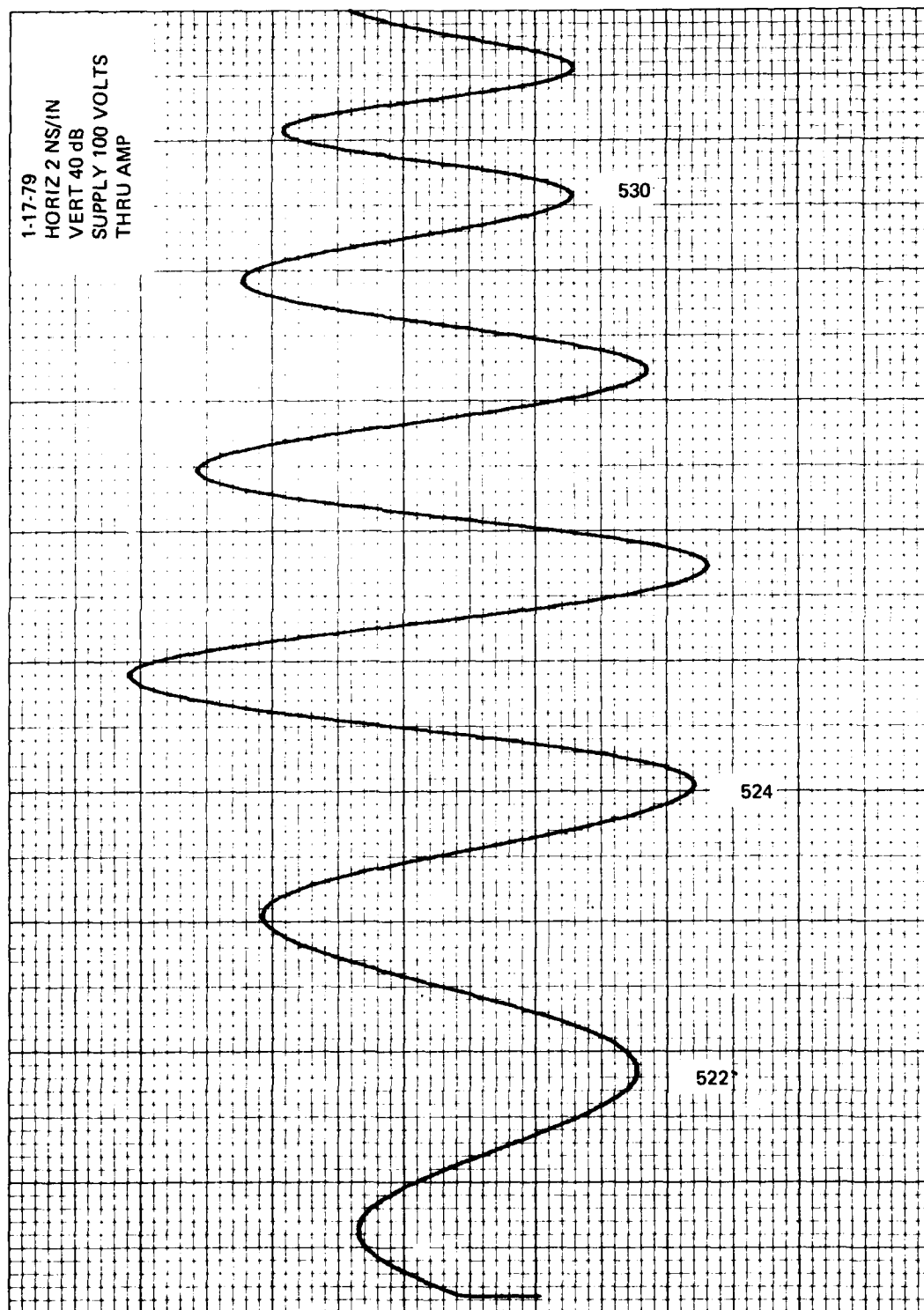


80 MV (X 100)
8 VOLTS

80 MV (X 100)
8 VOLTS

0

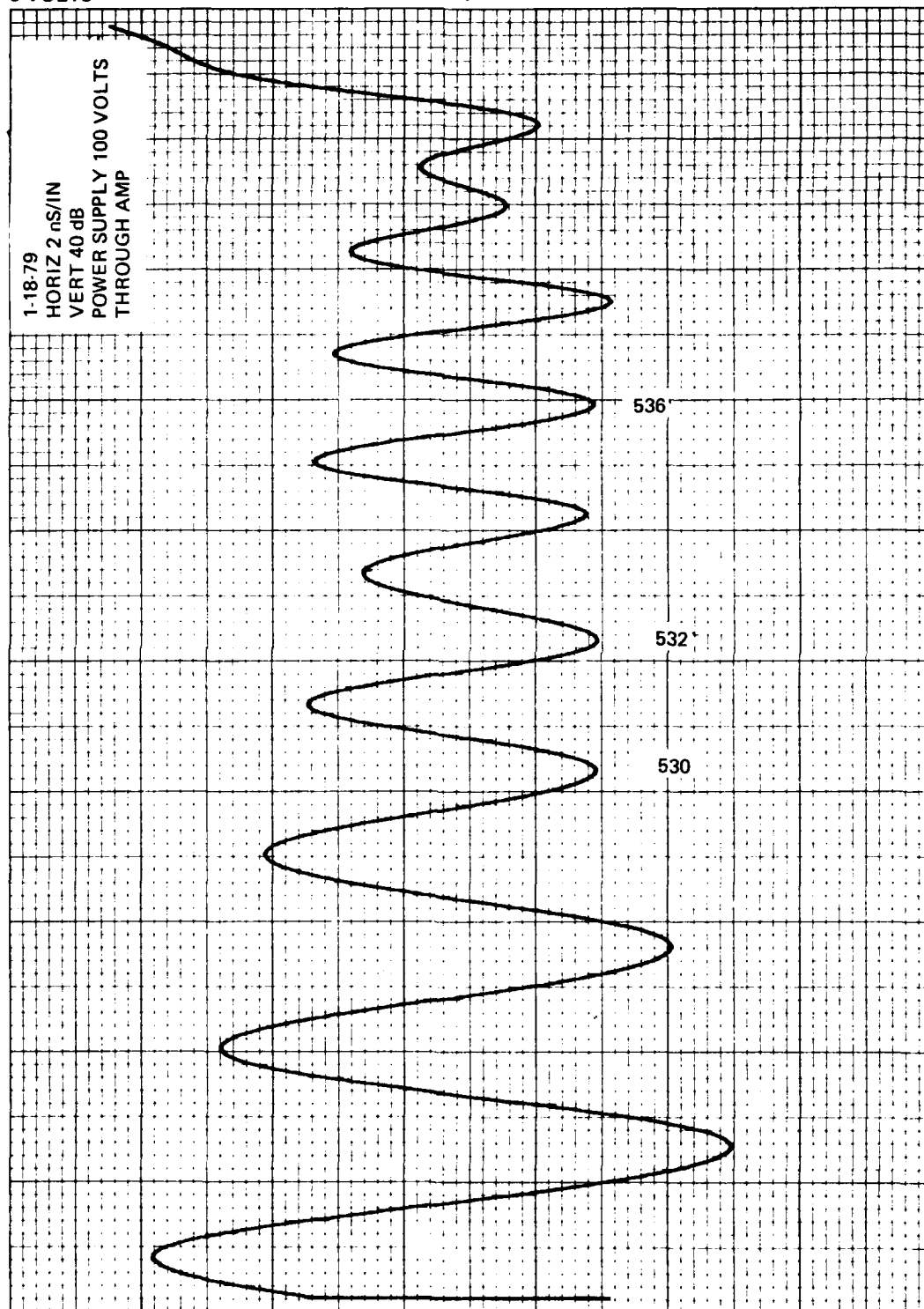
1-17-79
HORIZ 2 NS/IN
VERT 40 dB
SUPPLY 100 VOLTS
THRU AMP



8 MV (X 100)
8 VOLTS

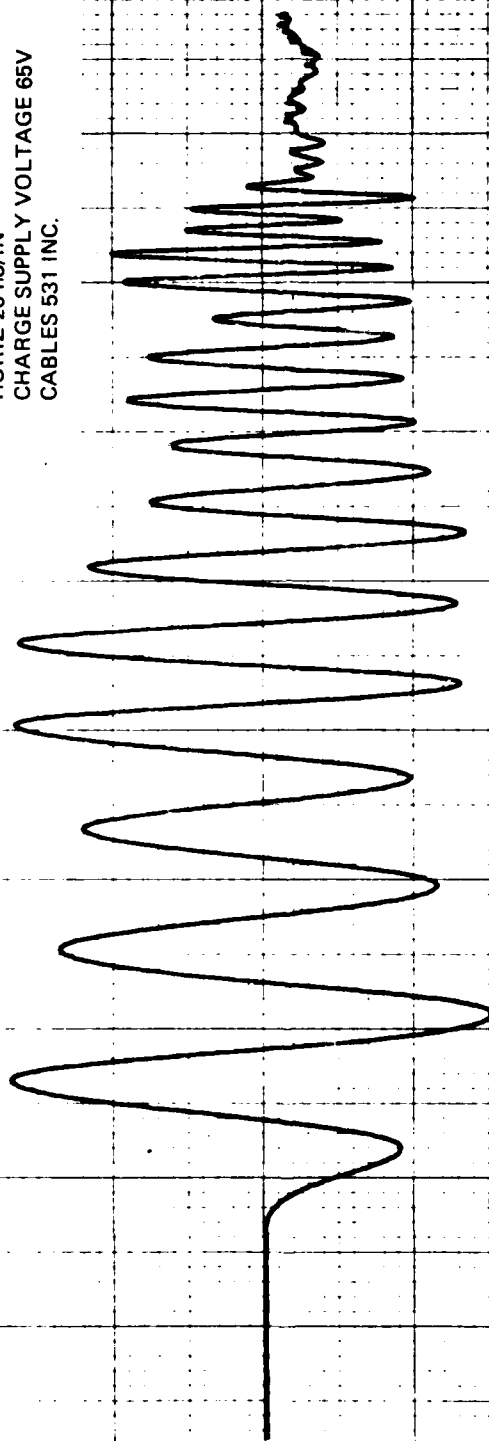
0

8 MV (X 100)
8 VOLTS

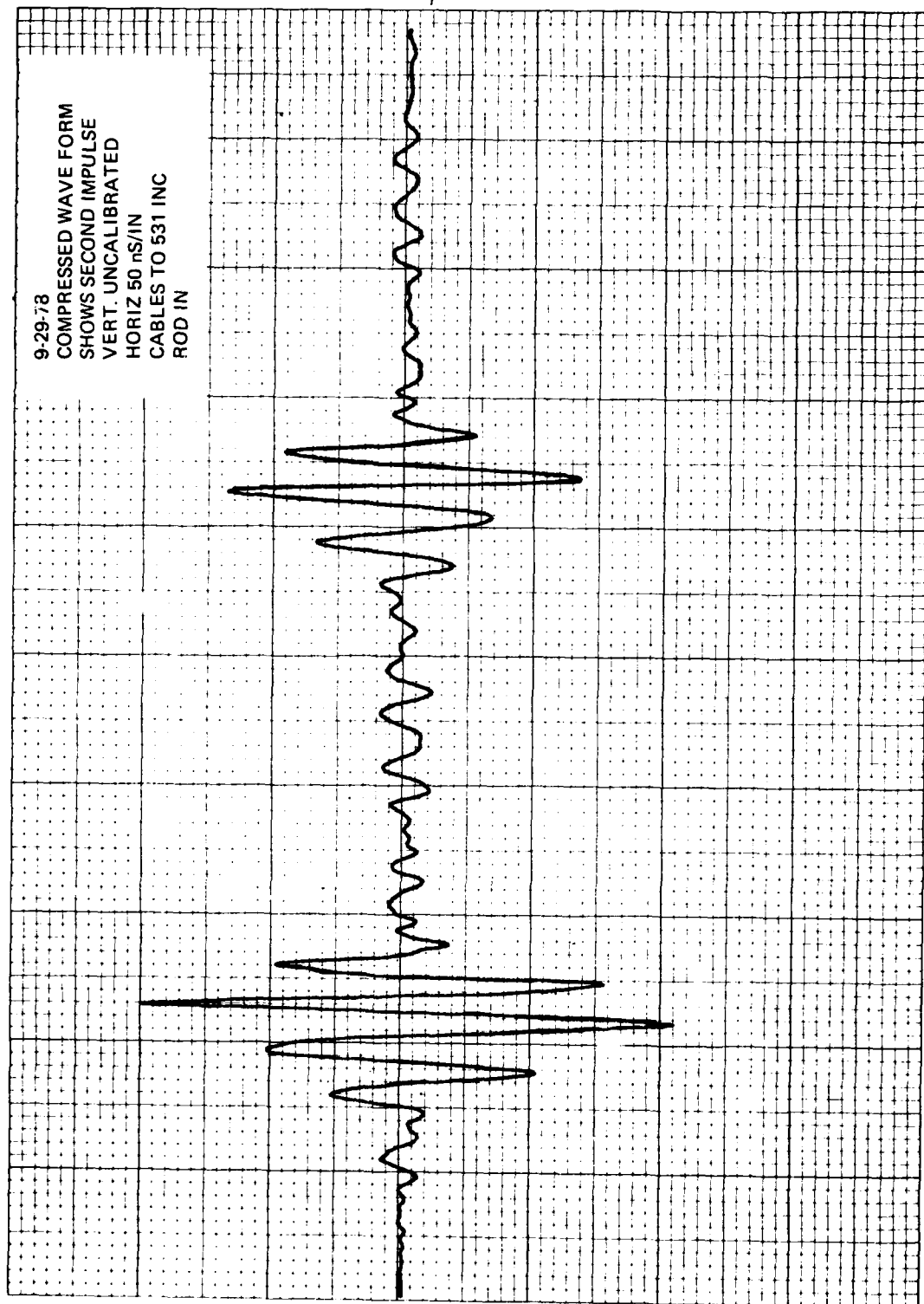


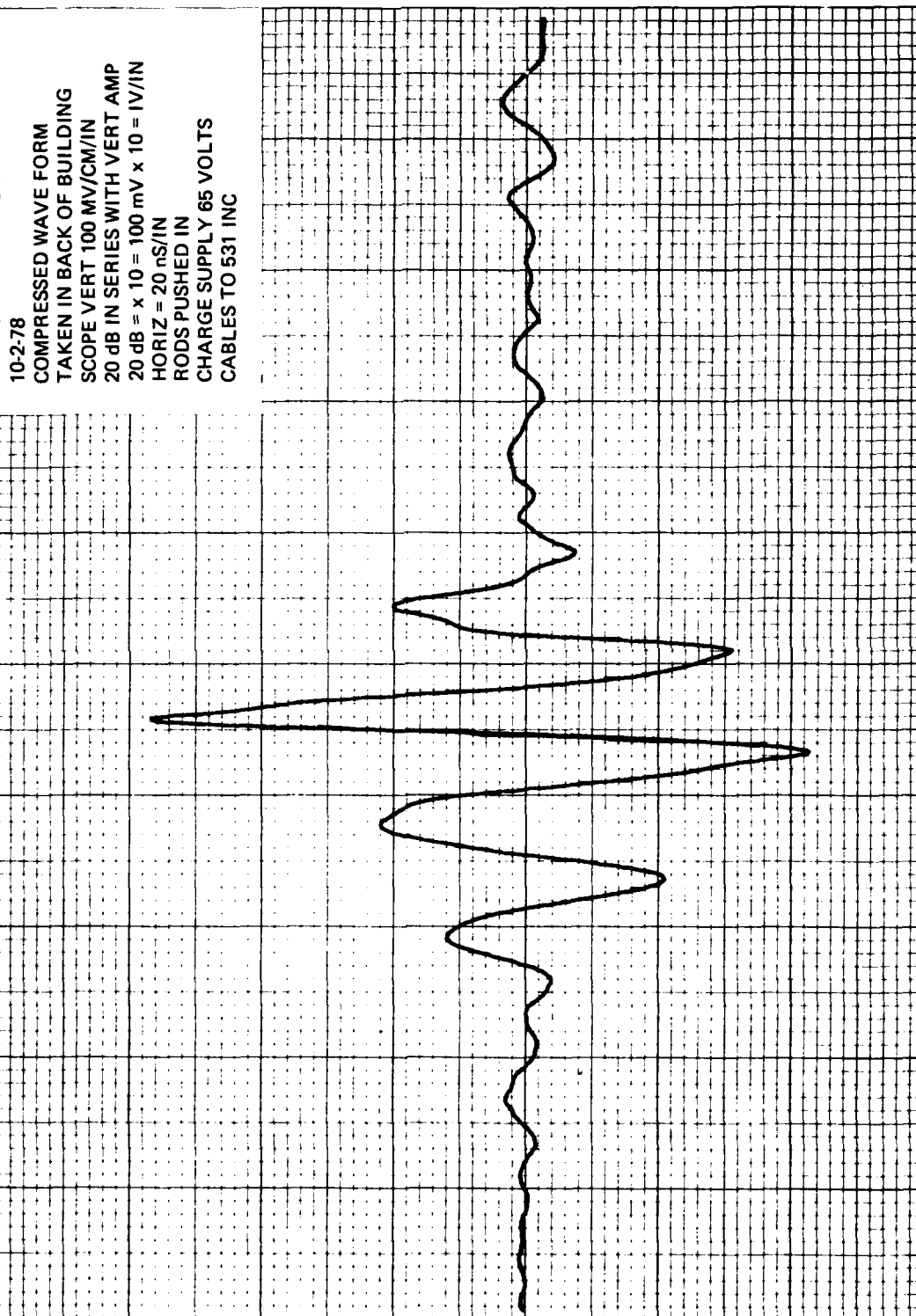
PRELIMINARY TESTING OF WAVEFORM GENERATOR,
EXCLUDING CABLES #532 TO #542.
2 OCTOBER 1978

10-2-78
WAVEFORM APPLIED TO ANTENNA
SCOPE VERT SET TO 50 MV/IN
40 dB IN SERIES WITH VERT IN.
40 dB = x 100
50 MV x 100 = 5000 mV - 5 V/IN
HORIZ 20 nS/IN
CHARGE SUPPLY VOLTAGE 65V
CABLES 531 INC.



9-29-78
COMPRESSED WAVE FORM
SHOWS SECOND IMPULSE
VERT. UNCALIBRATED
HORIZ 50 ns/IN
CABLES TO 531 INC
ROD IN

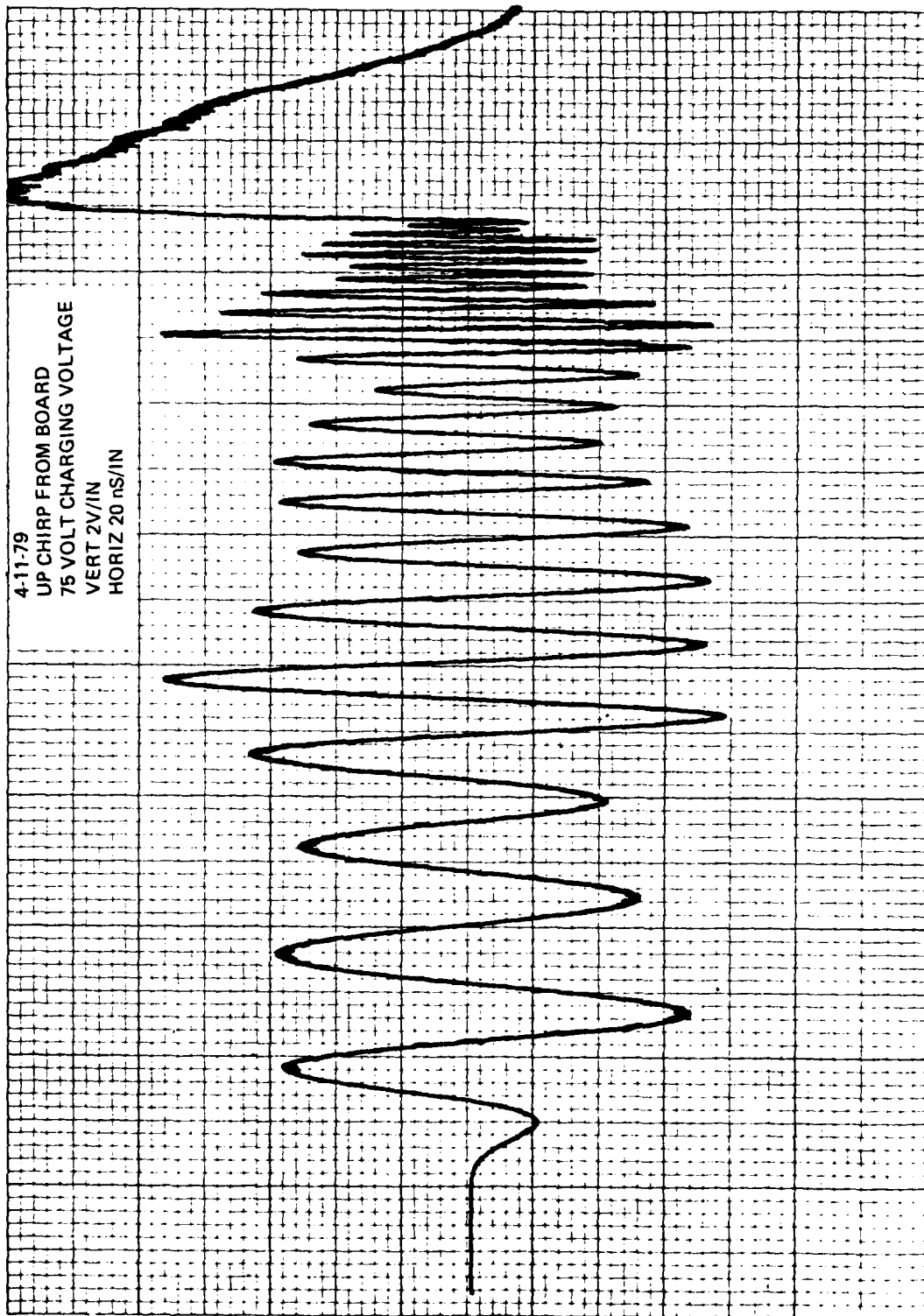


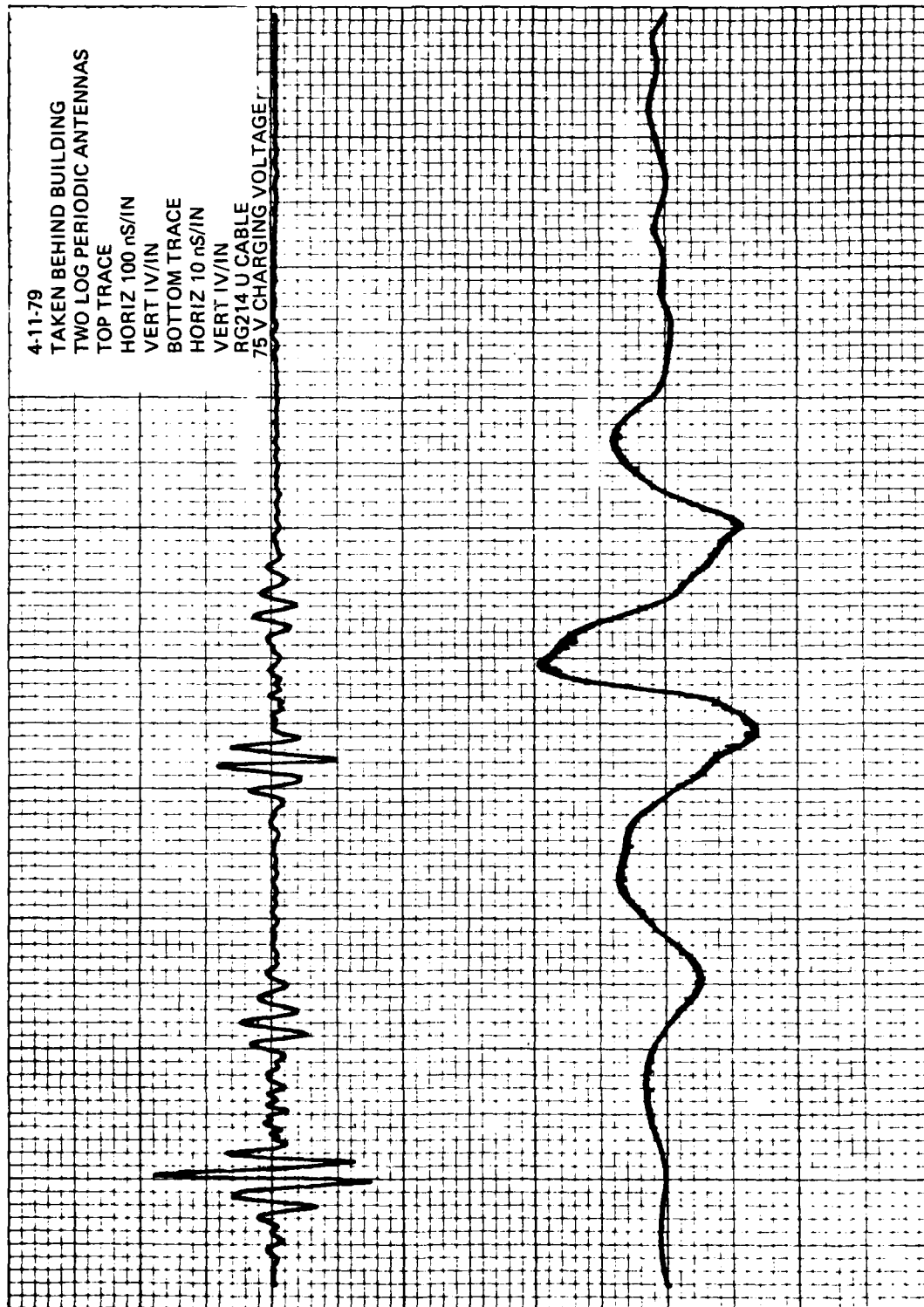


FINALIZED DATA ON RECONSTRUCTED PULSE TO INCLUDE:

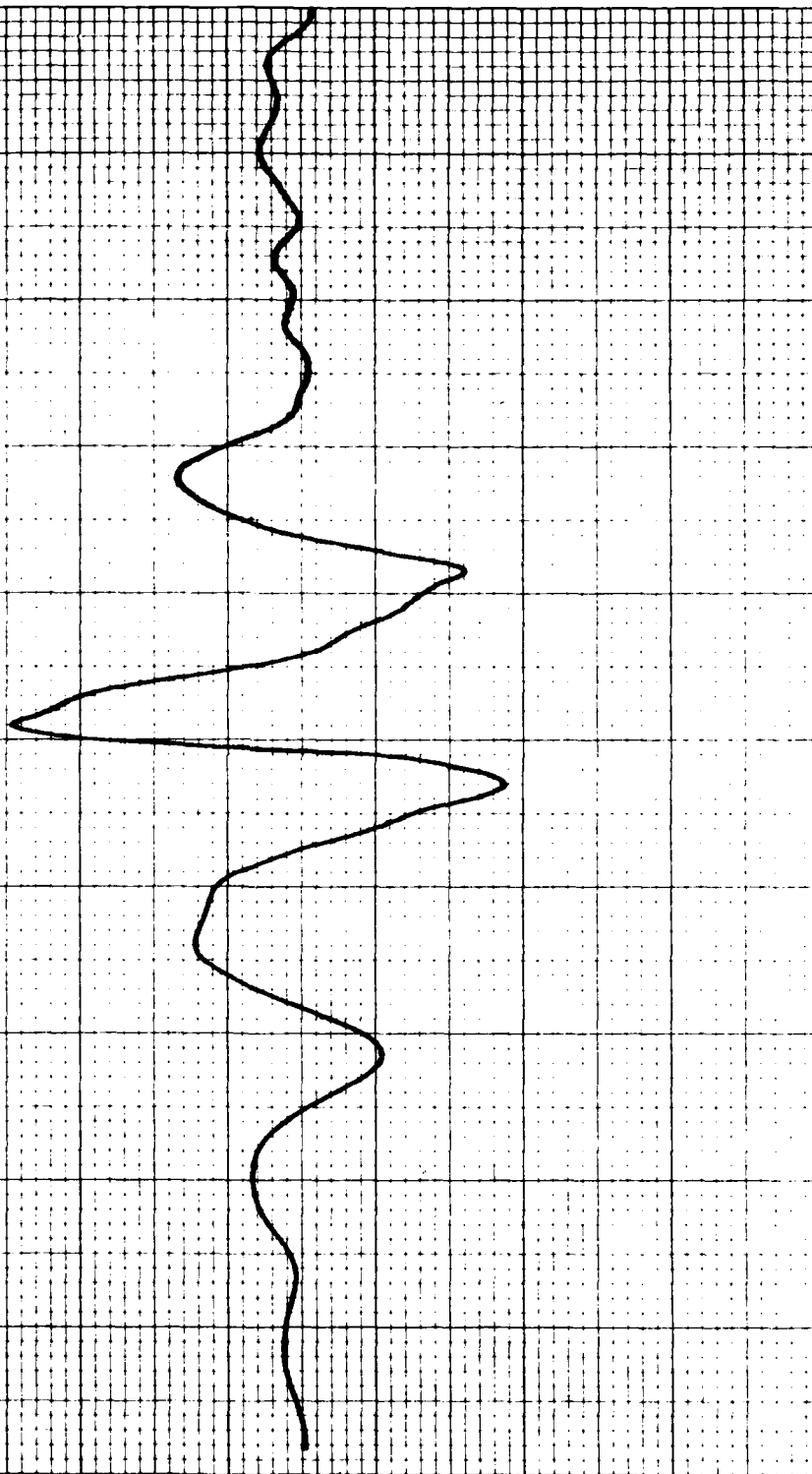
- 1. WAVEFORM GENERATOR OUTPUT AS SEEN AT THE ANTENNA.**
- 2. RECEIVED PULSE CHARACTERISTICS WITH EXPANDED VIEW.**
- 3. TEST INVOLVING A STUB MONOPOLE THAT SHOWS REFLECTIONS UNDER TWO DIFFERENT CONDITIONS.**

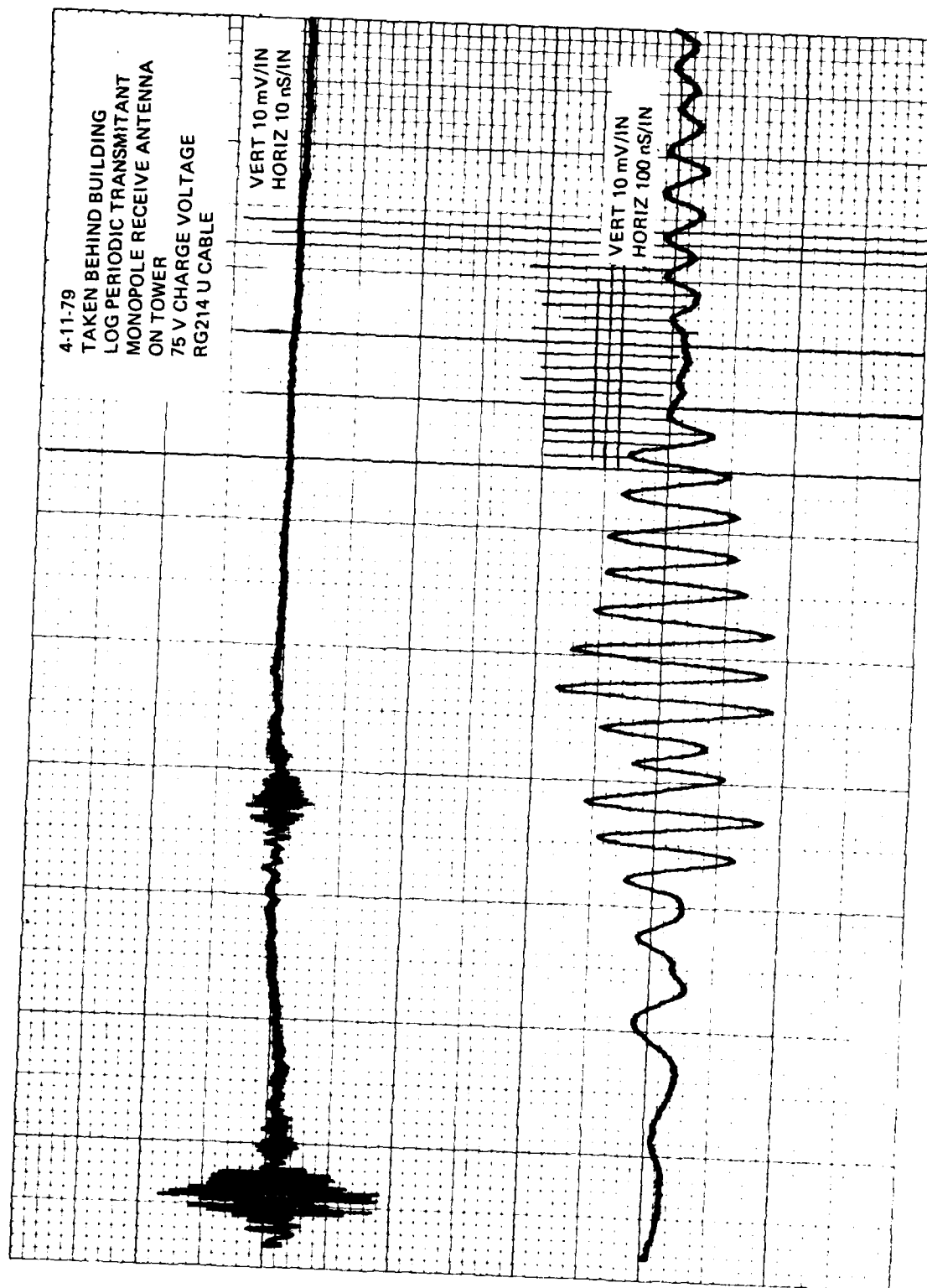
11 APRIL 1979



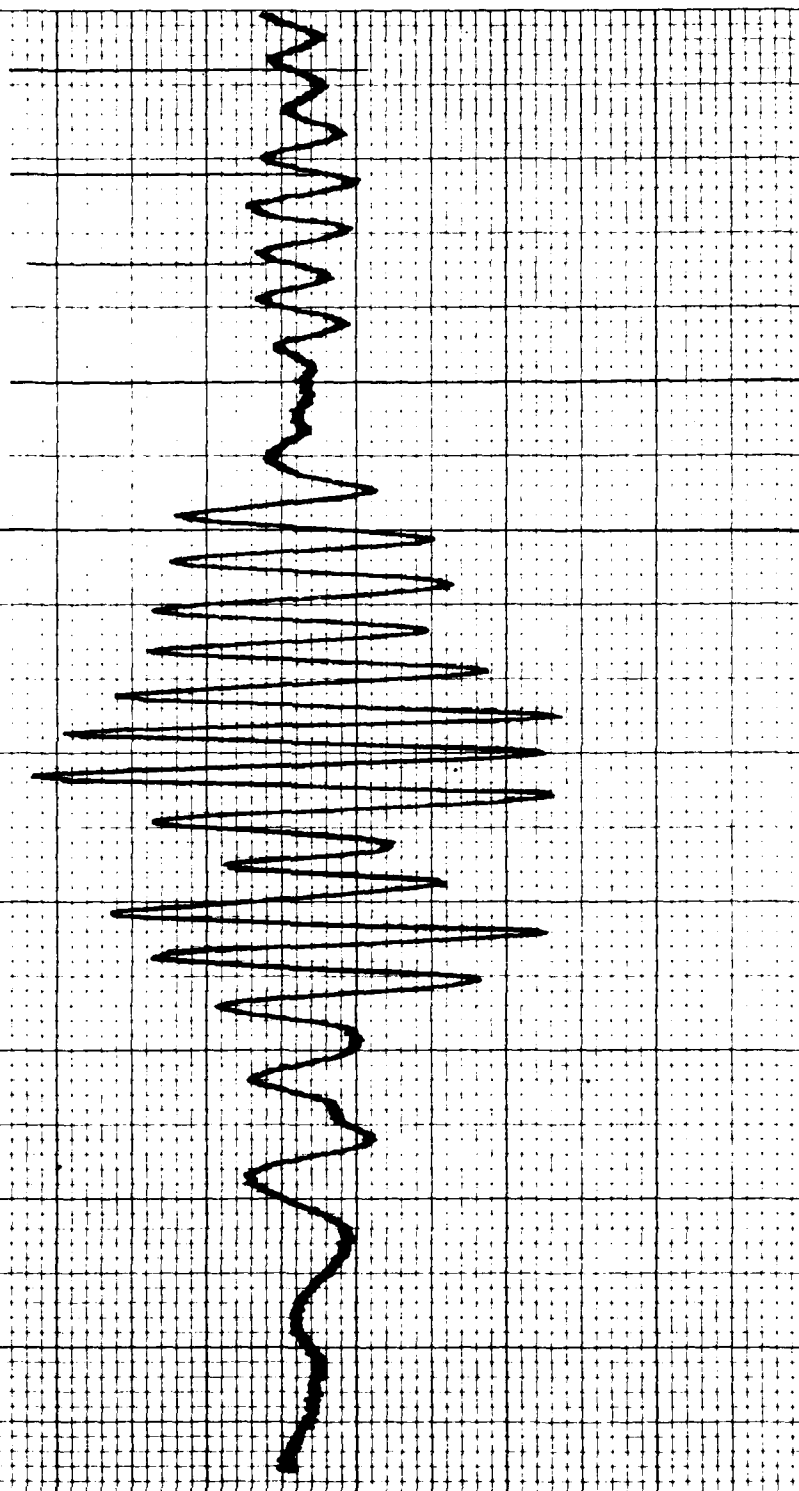


4-11-79
TAKEN BEHIND BUILDING
TWO LOG PERIODIC ANTENNAS
VERT 5V/IN.
HORIZ 10 nS/IN
75 VOLT CHARGING VOLTAGE
RG214 U CABLE

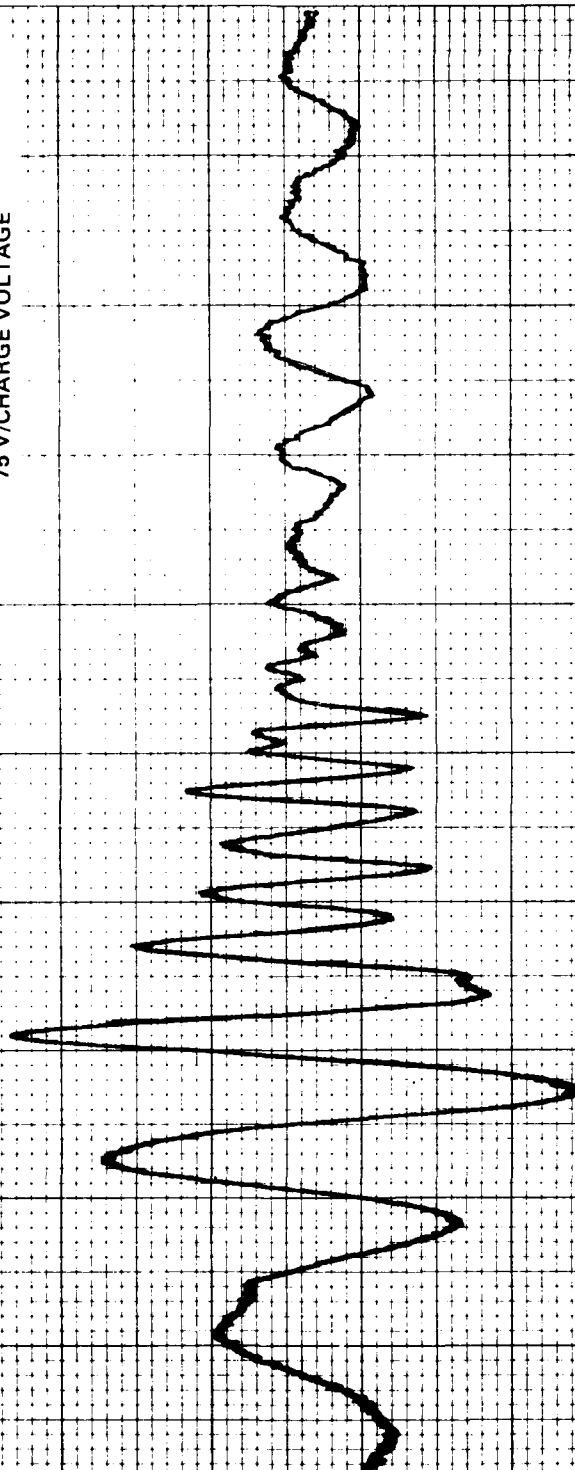




4-11-79
TAKEN BEHIND BUILDING
TRANSMIT ANTENNA LOG PERIODIC
RECEIVE ANTENNA MONOPOLE
ON TOWER
VERT 5 mV/IN
HORIZ 10 ns/IN
75 VOLT CHARGE VOLTAGE
RG214 U CABLE



4-11-79
TAKEN BEHIND BUILDING
TRANSMIT ANTENNA LOG PERIODIC
RECEIVE ANTENNA MONOPOLE
(HAND HELD)
VERT 5 mV/IN
HORIZ 10 ns/IN
RG214 U CABLE
75 V/CHARGE VOLTAGE



CONCLUSIONS

CONCLUSIONS

1. The processing gain of approximately 20 dB, as compared to CW signal, was obtained.
2. The processing gain does not deteriorate appreciably when antennas are misaligned.
3. The concept of utilizing two log-periodic antennas as matched filters appears to be valid.
4. The generator, as constructed, is extremely difficult to assemble and "tune" to produce the specified waveform. A different technique, perhaps using SAW devices trimmed by programmed machinery, can be adopted.

APPENDIX 1

**THEORY OF THE RECONCILIATION OF
SEVERAL SLIGHTLY DIFFERING
EMPIRICAL GRAPHS OF A
SINGLE, UNDERLYING LOGARITHMIC
DOWNCHIRP WAVEFORM**

APPENDIX 1

THEORY OF THE RECONCILIATION OF SEVERAL SLIGHTLY DIFFERING EMPIRICAL GRAPHS OF A SINGLE, UNDERLYING LOGARITHMIC DOWNCHIRP WAVEFORM

1. THEORETICAL FORMULAE

For a suitable choice of the time-origin, the time T , at which any specified number N of HALF-cycles (not necessarily an integer) will have occurred, is ideally expressible by means of the formula:

$$T = C K^N, \quad (1)$$

where C and K are suitable positive constants. This formula, if solved for N , has the form:

$$N = A \ln T - B, \quad (2)$$

where A and B are constants that are determinable from C and K via the formulas:

$$A = 1 / \ln K, \quad (3)$$

$$B = \ln C / \ln K, \quad (4)$$

whose own inverses are:

$$K = \exp(1/A), \quad (5)$$

$$C = \exp(B/A). \quad (6)$$

2. EMPIRICAL STATEMENT OF THE TIMES OF ZERO-CROSSINGS

We suppose that measurement of the positions of zero-crossings of the chirp waveform, on the various empirically obtained waveform graphs (chart-recorder outputs of sampling-scope information), together with the stated time calibration of each of the graphs, gives the following information:

t_{NM} , the time of occurrence of the N^{th} zero-crossing on the M^{th} graph, measured arbitrarily from the left-hand margin of the graph, is known for each graph (for a different range of N - values on each of the different graphs). (7)

In all the present work, times are uniformly assumed to be expressed in nsec.

3. REDUCTION OF THE EMPIRICAL TIMES BY SCALE-CHANGE AND ORIGIN-SHIFT

On the M^{th} graph, the "reduced time-coordinate," T_{NM} , corresponding to the "primary time-coordinate" t_{NM} of the N^{th} zero-crossing, is assumed to be obtainable from t_{NM} by the formula:

$$T_{NM} = S_M t_{NM} + D_M, \quad (8)$$

where S_M is a (not yet specified) scale factor which putatively (if different from unity) corrects the time calibration of the M^{th} graph; and D_M is similarly an unspecified corrective shift of the time origin, performed on the M^{th} graph after the time-scale correction S_M is applied.

The reduced zero-crossing times T_{NM} are assumed to be directly comparable with times calculated from the theoretical formula (1) (whereas the primary times, t_{NM} of the zero-crossings are not so comparable). NOTE: It is assumed throughout that a given N -value refers to the same zero-crossing of the underlying chirp waveform, regardless of which graph is being examined.

4. OFFSETS BETWEEN THE EMPIRICAL AND THE THEORETICAL ZERO-CROSSING TIMES

If the waveform in question were mathematically a perfect logarithmic downchirp, and were perfectly accurately portrayed by the various graphs, then one could expect to find (see the form of Eq. 1):

$$T_{NM} = C K^N \text{ (theoretical formula),} \quad (9)$$

--for suitable constants C and K that do not depend upon the graph M being examined, (and for suitable origin-shifts D_M (see Eq. 8) on the various graphs, and for no scale corrections (i. e., all the $S_M = 1$) on the various graphs).

However, in the absence of such ideal circumstances, Eq. (9) will in general not hold exactly at any measured point. It becomes of interest, therefore, to calculate

the amount by which Eq. (9) is not satisfied, at each measured point. This discrepancy, or offset, will be:

$$(T_{NM} - C K^N) \text{ units of time,} \quad (10)$$

at the N^{th} zero-crossing, on the M^{th} graph, where C and K are as yet unspecified constants.

5. NORMALIZATION OF THE TIME-OFFSETS

A given amount of time-offset (10) will of course have widely different significances, depending upon whether it refers to a zero-crossing located in a high-frequency or a low-frequency region of the chirp. Therefore, to compensate for this, and provide a measure for offset that will have a fixed significance at all locations in the chirp, the time-offset (10) will be expressed dimensionlessly, as a fraction of the chirp's instantaneous cycle-width, or, period, in the same locality.

By differentiating Eq. (1) to obtain dT/dN , the instantaneous rate of increase of time per HALF-cycle of the chirp waveform, one finds:

$$dT/dN = C K^N \ln K \text{ (in nsec/HALF-cycle).} \quad (11)$$

The instantaneous period of the chirp is therefore:

$$2C K^N \ln K \text{ (in nsec/full cycle).} \quad (12)$$

By dividing each time-offset (10) by the corresponding instantaneous period (12), one may therefore define the equivalent "offsets, in cycles of the chirp oscillation," as:

$$"E_{NM}" \equiv (T_{NM} - C K^N) / (2C K^N \ln K) \text{ cycles,} \quad (13)$$

at the N^{th} zero-crossing, on the M^{th} graph.

The offsets or discrepancies E_{NM} of (13) can be expressed more explicitly, in terms of the primary measured time-coordinates t_{NM} , by using Eq. (8) to eliminate the T_{NM} from (13); this gives the offset at the N^{th} zero-crossing, on the M^{th} graph, as:

$$E_{NM} = (S_M t_{NM} + D_M - C K^N) / (2C K^N \ln K), \quad (14)$$

measured in cycles of oscillation.

6. MINIMIZATION OF THE ZERO-CROSSING OFFSETS ON EACH GRAPH

A suitable measure of the over-all offset between the reduced empirical zero-crossings and the theoretical zero-crossings, on the M^{th} graph, is the sum of squares of the offsets (14) for that graph, i. e., the measure " P_M " defined by:

$$P_M \equiv \sum_N (E_{NM})^2, = (2C \ln K)^{-2} \sum_N [(t_{NM} K^{-N}) S_M + (K^{-N}) D_M - C]^2. \quad (15)$$

By expanding the sum in (15), one obtains:

$$\begin{aligned} P_M = (2C \ln K)^{-2} [& (S_M)^2 \sum_N (t_{NM})^2 K^{-2N} + 2S_M D_M \sum_N t_{NM} K^{-2N} \\ & + (D_M)^2 \sum_N K^{-2N} - 2CS_M \sum_N t_{NM} K^{-N} - 2CD_M \sum_N K^{-N} \\ & + C^2 J_M], \end{aligned} \quad (16)$$

where:

(" J_M " denotes the number of confidently measurable zero-crossings on the M^{th} graph.) (16 $\frac{1}{2}$)

Examination of (16) reveals that P_M is simply a quadratic function of the unknown scale factor S_M and of the unknown time-origin-shift D_M , for the M^{th} graph. P_M can therefore readily be minimized with respect to the choices of S_M and D_M , by equating to zero the partial derivatives $\partial P_M / \partial S_M$ and $\partial P_M / \partial D_M$; this yields (after canceling common constant factors) the following two simultaneous linear equations for S_M and D_M :

$$S_M \sum_N (t_{NM})^2 K^{-2N} + D_M \sum_N t_{NM} K^{-2N} = C \sum_N t_{NM} K^{-N}, \quad (17)$$

and

$$S_M \sum_N t_{NM} K^{-2N} + D_M \sum_N K^{-2N} = C \sum_N K^{-N}. \quad (18)$$

The solution of the simultaneous equations (17) and (18), for the optimum S_M and D_M (that minimize P_M of (15)), is:

$$D_M = Q_M C, \quad (19)$$

and

$$S_M = R_M C, \quad (20)$$

where Q_M and R_M stand for the following readily calculated, but complicated-appearing quantities:

$$Q_M \equiv \left[\frac{\sum_N (t_{NM})^2 K^{-2N} \sum_N K^{-N} - \sum_N t_{NM} K^{-2N} \sum_N t_{NM} K^{-N}}{\sum_N (t_{NM})^2 K^{-2N} \sum_N K^{-2N} - (\sum_N t_{NM} K^{-2N})^2} \right], \quad (21)$$

and

$$R_M \equiv \left[\frac{\sum_N (t_{NM} K^{-N}) \sum_N K^{-2N} - \sum_N t_{NM} K^{-2N} \sum_N K^{-N}}{\sum_N (t_{NM})^2 K^{-2N} \sum_N K^{-2N} - (\sum_N t_{NM} K^{-2N})^2} \right], \quad (22)$$

which refer to, and are obtained from, the M^{th} graph, as the suffixes imply.

When the optimum values (19) and (20) are substituted for D_M and S_M in Eq. (16), and the resulting expression is simplified with the aid of Eq. 's (17) and (18), the minimized value for P_M is found to be:

$$P_M \text{ (minimum)} = \left[\frac{J_M - Q_M \sum_N K^{-N} - R_M \sum_N t_{NM} K^{-N}}{(2 \ln K)^2} \right], \quad (23)$$

which does not depend upon the value assigned to C .

7. MINIMIZATION OF THE REQUIRED TIME-SCALE CORRECTIONS

The scale-change or scale-"correction" factors S_M for the various graphs would most ideally all be equal to unity. But Eq. (20) imposes a constraint which prevents this from taking place, in general. It therefore becomes of interest to evaluate how close to unity Eq. (20) permits the various S_M to be chosen; and it is important, here, to notice that the constant parameter "C" in (20) has not yet been assigned, and is available for optimization.

The amount by which a given scale factor S_M differs from unity is, with use of Eq. (20):

$$(S_M - 1) = (R_M C - 1). \quad (24)$$

The sum of the squares of these differences may then be taken, over the various graphs, with weights that are taken to be the numbers of confidently measured zero-crossings on the respective graphs, J_M (see (16 $\frac{1}{2}$)). The weighted sum of interest is thus:

$$''W'' \equiv \sum_M J_M (S_M - 1)^2 = \sum_M J_M (R_M C - 1)^2. \quad (25)$$

The minimization of this weighted sum brings the scale factors S_M as close to unity as the internal consistency of the zero-crossing-time data permits, and thus minimizes the severity of the assumptions that one needs to make concerning the inaccuracies of the stated time calibrations, in order to have the data jibe with the assumption that the separate graphs arise from a single logarithmic-downchirp waveform.

By expanding the last sum in Eq. (25), one finds:

$$W = C^2 \sum_M J_M (R_M)^2 - 2C \sum_M J_M R_M + J, \quad (26)$$

where

$$''J'' \equiv \sum_M J_M \quad (27)$$

is the total number of confidently measured zero-crossings on all the graphs involved. But W of Eq. (26) is simply a quadratic function of the unassigned parameter C , and therefore is readily shown to be minimized by the following choice of C :

$$C = (\sum_M J_M R_M) / (\sum_M J_M (R_M)^2), \quad (28)$$

whose numerical value is easily found with the aid of Eq. (22). And, when the choice (28) is made for C , the minimized value of the weighted sum W of (25) or (26) is found to be:

$$\begin{aligned} W \\ \text{(minimum)} \end{aligned} = \left[J - \left((\sum_M J_M R_M)^2 / (\sum_M J_M (R_M)^2) \right) \right]. \quad (29)$$

8. DEFINITION OF RMS ERROR MEASURES

The sums of squares (of the number-of-cycle offsets between reduced empirical zero-crossings and theoretical zero-crossings) P_M , defined in (15) for any given graph, and minimized in Eq. (23), can themselves be summed over all the various

graphs, and the resulting over-all sum can be divided by the total number of measured zero-crossings, J of Eq. (27), to obtain a mean-square number-of-cycles offset for all the zero-crossings; this can then be square-rooted, to define an over-all RMS offset, E , in number of cycles, for all of the measured zero-crossings. Thus, we define the "RMS Offset," E , by:

$$E = \left[(1/J) \sum_M (\text{minimum } P_M \text{ from Eq. 23}) \right]^{1/2}, \quad (30)$$

measured in cycles of oscillation. By substituting from Eq. (23), this becomes:

$$E = (2 \ln K)^{-1} \left[1 - J^{-1} \sum_M (Q_M \sum_N K^{-N} + R_M \sum_N t_{NM} K^{-n}) \right]^{1/2}, \quad (31)$$

(expressed in cycles of oscillation), which is readily evaluated via (21) and (22).

In a similar way, an irreducible RMS amount, "U", by which the time-calibrations of the various graphs must be regarded as being uncertain and in need of correction by scale-factors differing from unity as discussed in Section 7, can be defined as the square-root of the weighted sum of squares W of (25), after W is minimized and divided by J , the total number of measured zero-crossings. Thus, the quantity U is defined by:

$$U \equiv \left[(1/J) (\text{minimum } W \text{ from Eq. 29}) \right]^{1/2}, \quad (32)$$

and represents the minimum weighted-RMS fractional adjustment that must be allowed, for time-scale recalibrations that are needed to bring the different waveform graphs' zero-crossing data into maximum accord with one another and with the conceptual picture of a single underlying downchirp waveform. Explicit use of Eq. (29) reduces Eq. (32) to the form:

$$U = \left[1 - \left(\sum_M J_M R_M \right)^2 \left(J \sum_M J_M (R_M)^2 \right)^{-1} \right]^{1/2}, \quad (33)$$

which can be numerically evaluated via (22). The units of U are "fractional adjustment of time-scale."

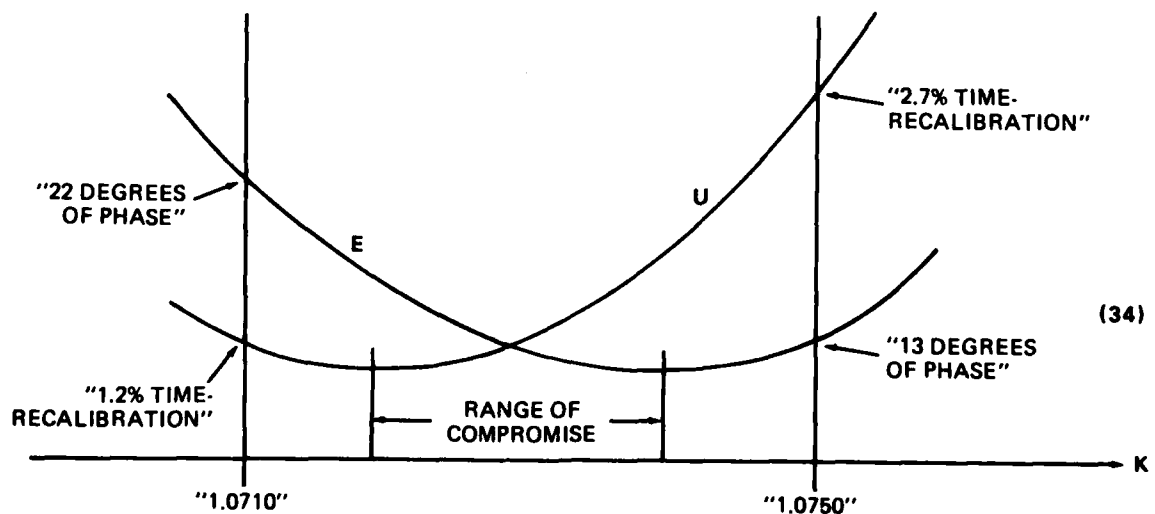
9. SUMMARY OF CALCULATION PATHWAYS

- A. To obtain the best adjustment or "reduction" of the measured zero-crossing times t_{NM} , use the sequence of equations (21), (22), (28), (19), (20), (8), to find the "empirical" times T_{NM} .
- B. To find the theoretical zero-crossings corresponding to these, use the sequence of equations (22), (28), (9).
- C. To find "U", the minimum weighted-RMS time-scale adjustment that is needed, over the various graphs, use the sequence of equations (22), (33).
- D. To find "E", the minimum RMS cycle-offset between the empirical and theoretical zero-crossings, for all the graphs, use the sequence of equations (21), (22), (31).

10. OPTIMIZATION OF THE CONSTANT PARAMETER "K" (the "log-change" factor per half-cycle)

By inspecting the calculation pathways just listed in Section 9, it becomes apparent that K is the only parameter that has so far remained undetermined. It cannot be obtained analytically, but instead must be found by numerical trial and error, as follows:

Versus different assumed values of K, calculate the values of U and E given by (33) and (31) (see Section 9, parts C. and D.); imagine the resulting U and E to be plotted versus K as sketched below:



The range of K , between the (in general, distinct) values of K that minimize U or E , will generally be small; and the U - and E -curves will generally be very flat in that "range of compromise"; K can then be taken to be at a convenient point in that range; after which, the optimized values of all the other parameters are determinable via the routes summarized in Section 9. The numbers used in the above sketch, while only illustrative, have been chosen to approximate actual results discussed in the main text.

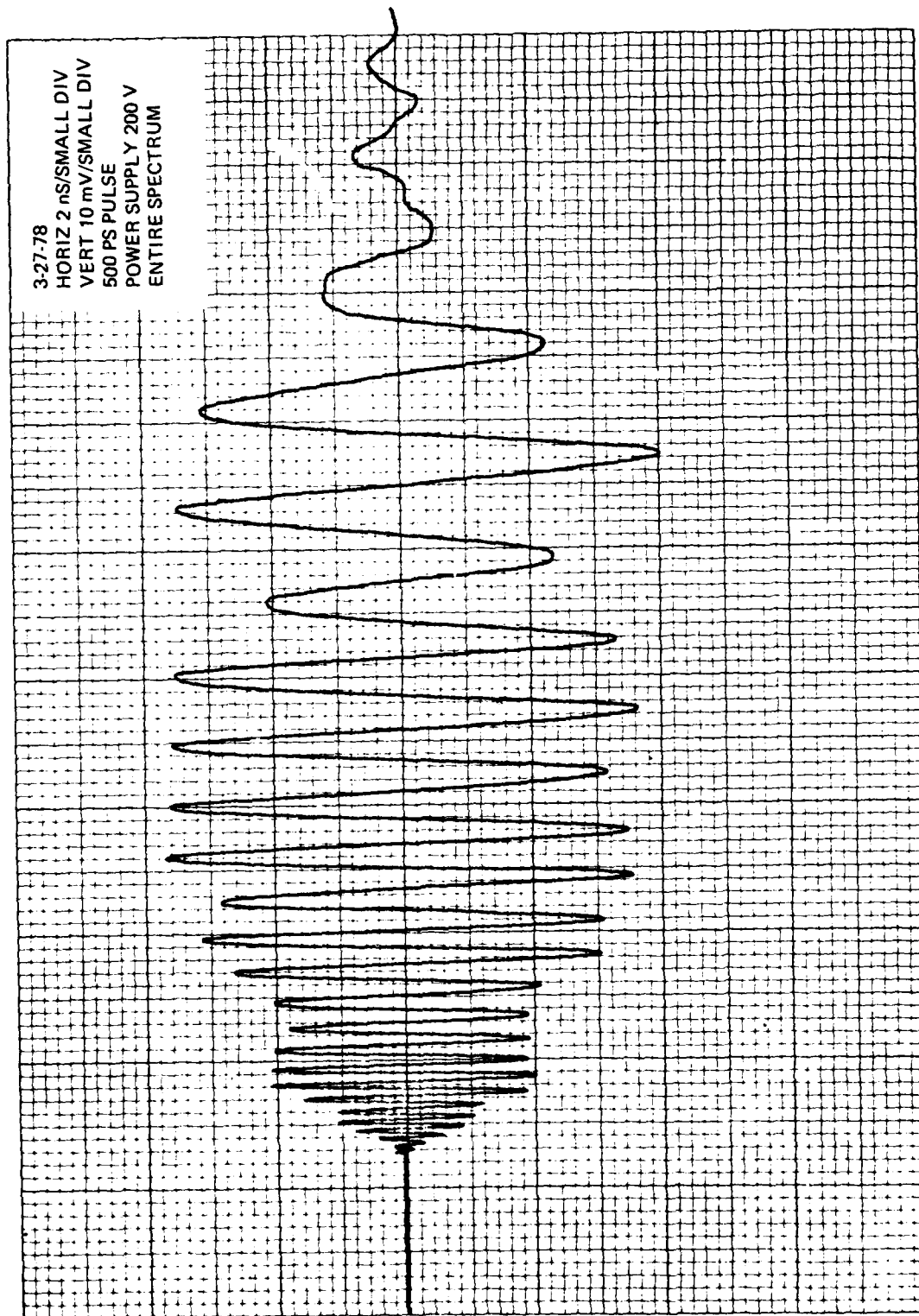
APPENDIX 2

**WAVEFORM GRAPHS RECENTLY
OBTAINED, SHOWING PORTIONS
OF THE COMBINED IMPULSE
RESPONSE OF TWO AEL
COPLANAR LOG-PERIODIC
ANTENNAS, TYPE APN-995B**

APPENDIX 2

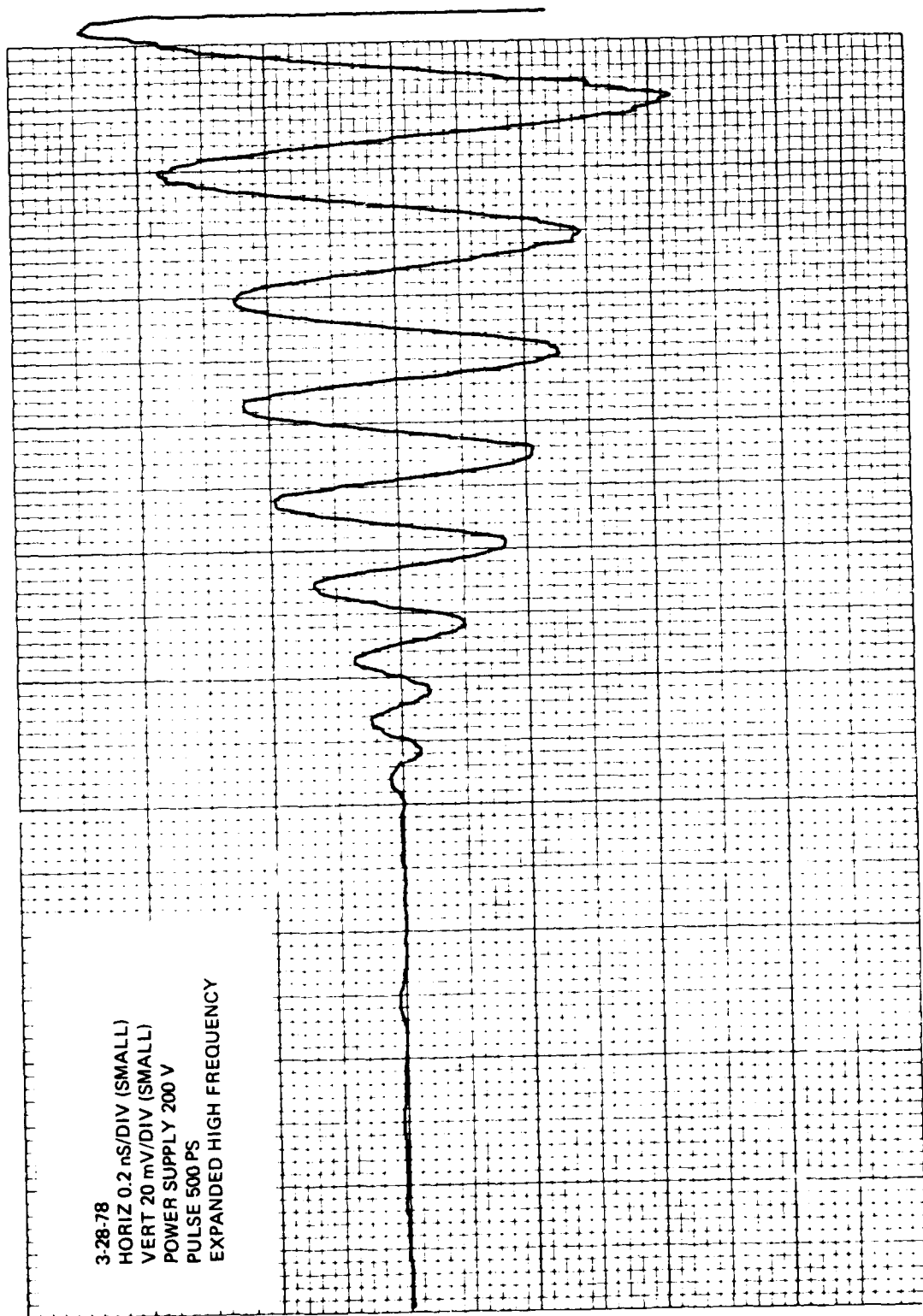
WAVEFORM GRAPHS RECENTLY OBTAINED, SHOWING PORTIONS
OF THE COMBINED IMPULSE RESPONSE OF TWO AEL COPLANAR
LOG-PERIODIC ANTENNAS, TYPE APN-995B

<u>Graph No.</u>	<u>Sweep Rate Involved</u> <u>(nsec/inch)</u>	<u>Zero-Crossings of Interest</u> <u>for Data Reduction</u>
2	20	#8 to #47
4	2	#1 to #16
5	10	#0 to #37
6	10	#28 to #46
7	10	#39 to #47

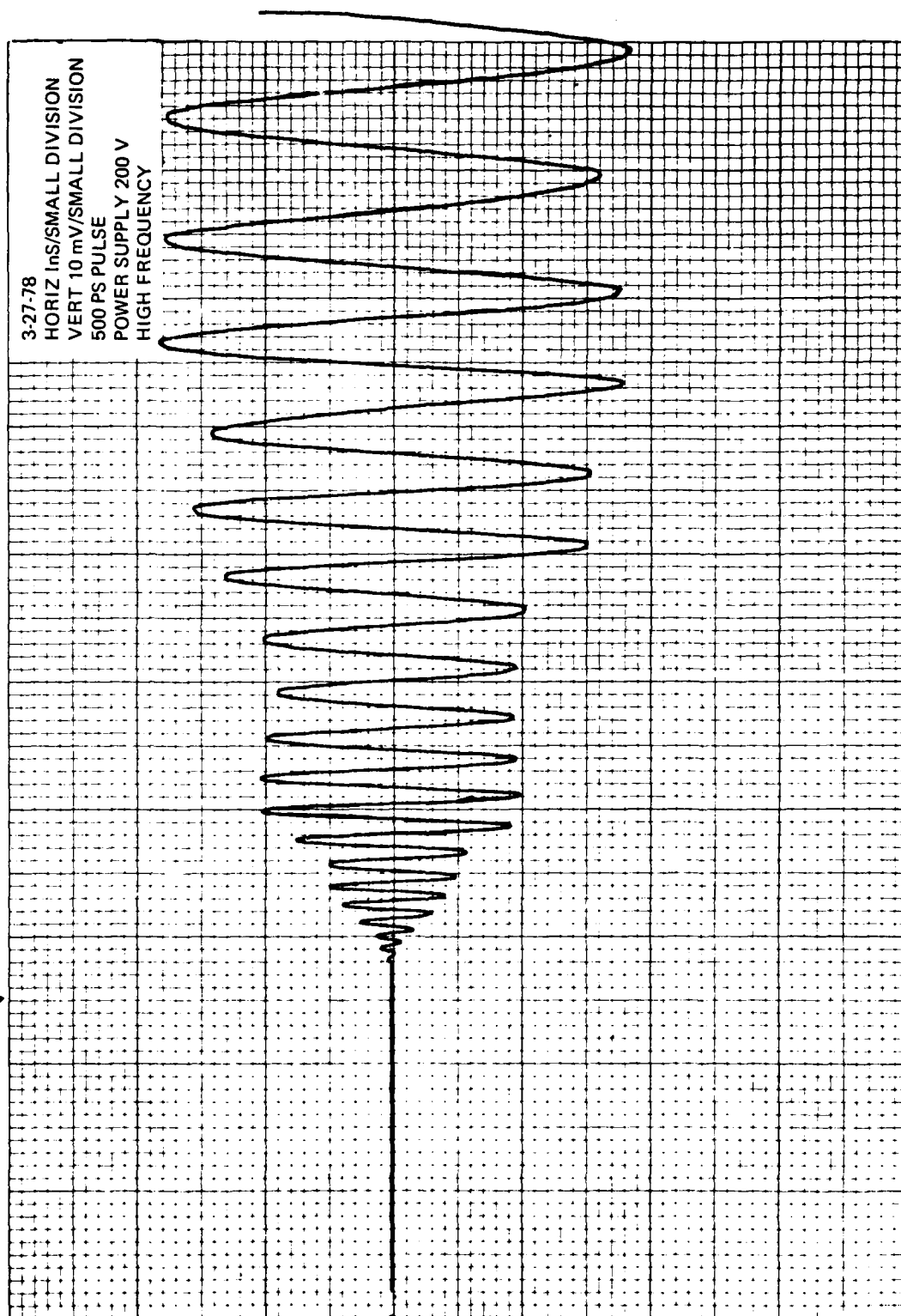


Graph 2

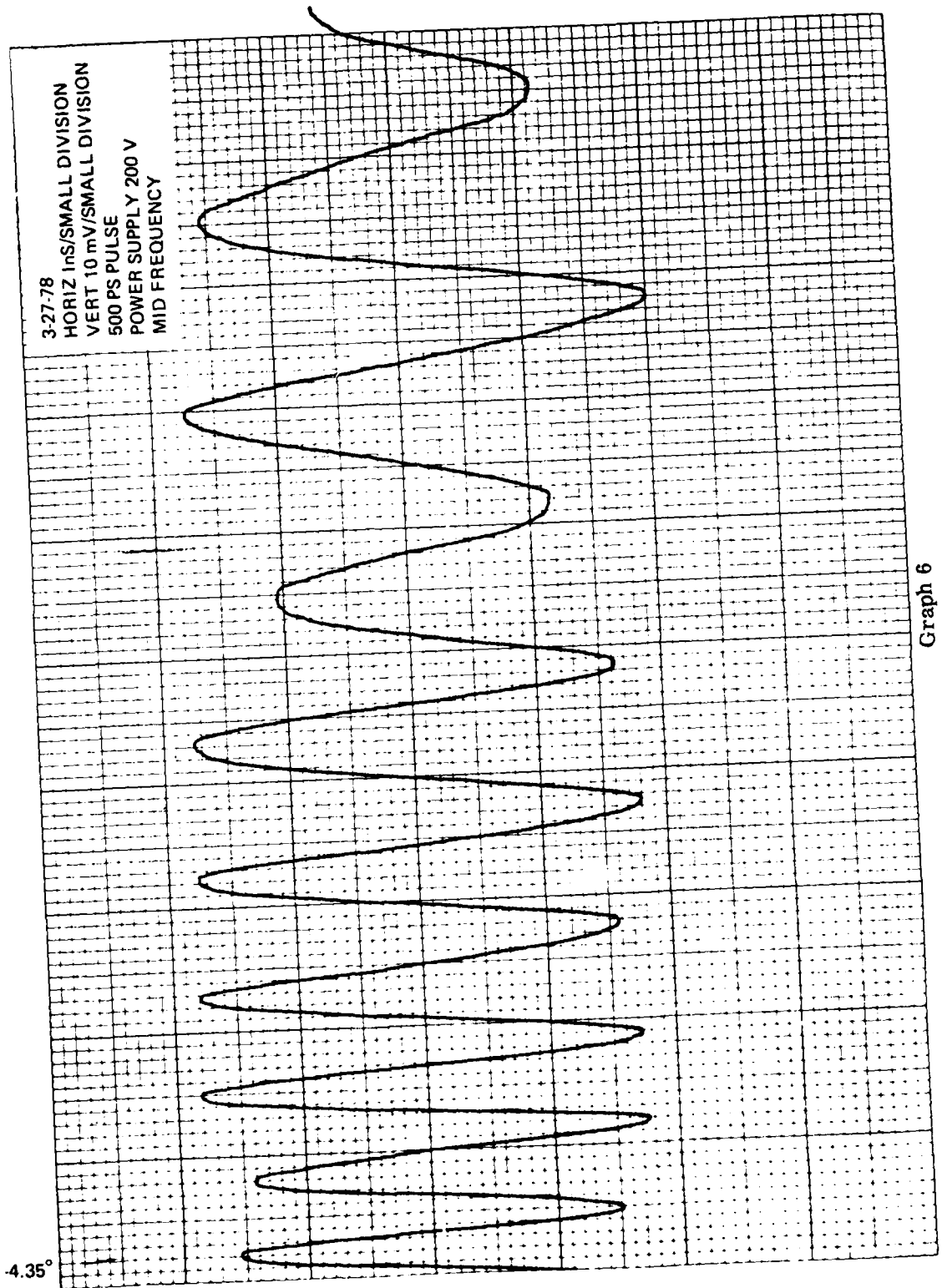
3-28-78
HORIZ 0.2 ns/DIV (SMALL)
VERT 20 mV/DIV (SMALL)
POWER SUPPLY 200 V
PULSE 500 PS
EXPANDED HIGH FREQUENCY



Graph 4

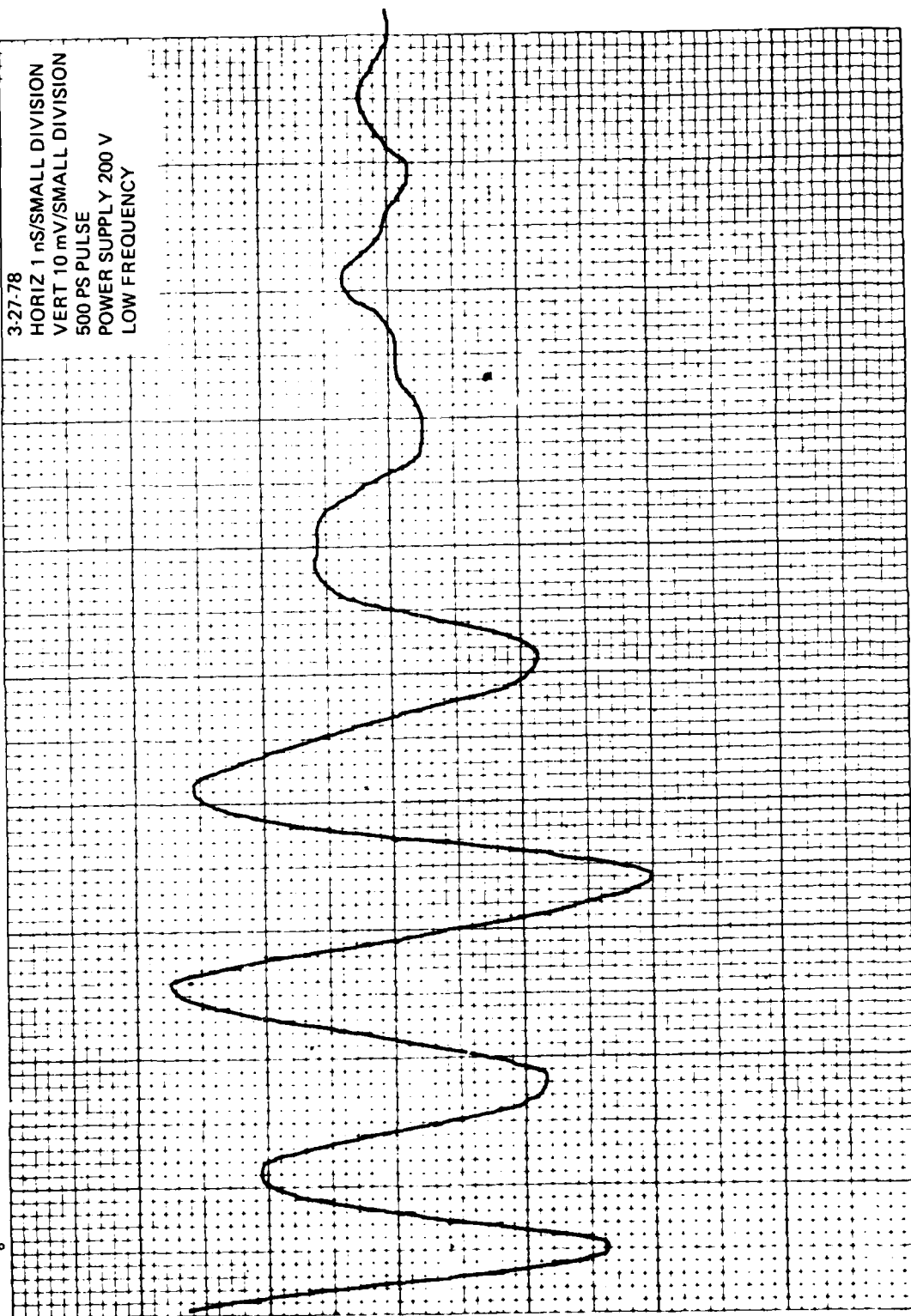


Graph 5



Graph 6

-9.00°



Graph 7

APPENDIX 3

**RELEVANT COMPUTER
PRINTOUT SHEETS**

This section intentionally omitted. May be obtained by contacting
Project Engineer (see DD 1473).

APPENDIX 4
COMPUTER MODELING
OF A
LOG-PERIODIC ANTENNA

COMPUTER MODELING OF A LOG-PERIODIC ANTENNA

Fred J. Deadrick

December 5, 1977

Work performed under the auspices of the U.S. Department of
Energy by the UCLLL under contract number W-7405-ENG-48



NOTICE

"This report was prepared as an account of work sponsored by the United States Government. Neither the United States nor the United States Department of Energy, nor any of their employees, nor any of their contractors, subcontractors, or their employees, makes any warranty, express or implied, or assumes any legal liability or responsibility for the accuracy, completeness or usefulness of any information, apparatus, product or process disclosed, or represents that its use would not infringe privately-owned rights."

NOTICE

Reference to a company or product name does not imply approval or recommendation of the product by the University of California or the U.S. Department of Energy to the exclusion of others that may be suitable.

Printed in the United States of America

Available from
National Technical Information Service
U.S. Department of Commerce
5285 Port Royal Road
Springfield, VA 22161
Price: Printed Copy \$: Microfiche \$3.00

Page Range	Domestic Price	Page Range	Domestic Price
001-025	\$ 4.00	326-350	\$12.00
026-050	4.50	351-375	12.50
051-075	5.25	376-400	13.00
076-100	6.00	401-425	13.25
101-125	6.50	426-450	14.00
126-150	7.25	451-475	14.50
151-175	8.00	476-500	15.00
176-200	9.00	501-525	15.25
201-225	9.25	526-550	15.50
226-250	9.50	551-575	16.25
251-275	10.75	576-600	16.50
276-300	11.00	601-up	1
301-325	11.75		

¹ Add \$2.00 for each additional 100 page increment from 601 pages up.

Distribution Category
UC-37



LAWRENCE LIVERMORE LABORATORY
University of California Livermore, California 94550

UCRL-52372

COMPUTER MODELING OF A LOG-PERIODIC ANTENNA

Fred J. Deadrick

MS. date: December 5, 1977

PREFACE

The work reported in this document was supported by the Defense Nuclear Agency under Subtask R99QAXE B075.

CONTENTS

Abstract	1
Introduction	1
Model Theory	1
Modeling Antenna Structure	1
Modeling Antenna Response	2
Modeling Transient Response	2
Results	3
Input Impedance	3
Transfer Functions	3
Transient Response	3
A Practical Example: EMP Transient Response	4
Conclusions	8
Acknowledgments	8
References	9

COMPUTER MODELING OF A LOG-PERIODIC ANTENNA

ABSTRACT

A computer model of a six-element log-periodic antenna is described and operated in both the time and frequency domains to calculate antenna input impedance, forward and backward incident-field transfer functions, and transient response characteristics. Computed results are compared with experimental test data to demonstrate the model's reliability. Additionally, the model is used to assess the antenna's coupling to an incident EMP wave to provide a practical illustration of the model's utility and to indicate its potential for further development.

INTRODUCTION

Until recent years, the state-of-the-art of computer simulation of electromagnetics systems was too primitive to permit the investigation of equipment behavior under a suitably broad range of conditions. Testing and optimizing an antenna, for example, required lengthy field testing and analysis of instrument data. Now, however, modeling techniques have advanced to the point where accurate models of complex structures are feasible. Accord-

ingly, I have applied a number of well-known numerical procedures to model a multi-element log-periodic antenna array in the presence of a finitely conducting ground and have compared computed behavior with experimental test results. In this report, I describe the theoretical foundation of the model, present results of measured vs theoretical data comparisons, and illustrate with an example how the model can be put to practical use.

MODEL THEORY

The antenna I selected is the U. S. Army model AS-2169/G, a six-element horizontal log-periodic dipole array (see Fig. 1). It is a typical broad-band communications antenna designed to operate in the 30- to 76-MHz range. Additionally, there is substantial experimental test data available for the antenna.¹

Modeling the behavior of a log-periodic antenna involves solving three sets of related problems: developing an adequate representation of the structure of the antenna, computing antenna response across the spectrum of its active bandwidth, and, finally, determining the antenna's transient response to an arbitrary waveform.

Modeling Antenna Structure

Modeling the structure of the log-periodic antenna calls for treating the antenna as an array of thin wires (i.e., where the maximum transverse dimension is small compared with the wire length and wavelength) and using a frequency-domain formulation of the thin-wire electric field integral equation.^{2,3} The numerical procedure involves representing a given wire contour with a series of piecewise linear segments. The unknown current on each segment used to model the structure is first expressed by a three-term-basis function (constant,

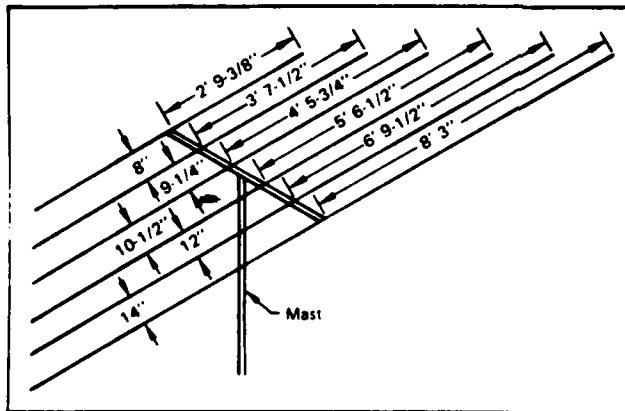


Fig. 1. Configuration and dimensions. Model AS-2169/G log-periodic antenna.

sine, and cosine), which is then simplified by an extrapolation procedure to reduce the number of unknowns to one per segment. Subsequently, delta-function weights are used to point-match the thin-wire integral equation at the segment centers. The result is a linear system whose order equals the number of segments in the model.

For the AS-2169/G antenna, the approximation procedure led to a model consisting of a series of 72 interconnected straight-wire segments or vectors (see Fig. 2). Each segment represents an unknown sample point in the moment-method solution of the electric field integral equation. (The arrowheads indicate the reference direction for positive current flow.)

In addition to the log-periodic element modeling, simulating the antenna structure also calls for representing the feedline connecting the six dipoles. This problem is solved by using a nonradiating transmission line equation with an impedance of 130 Ω , which closely approximates the boom impedance of the AS-2169/G. Between the dipole elements the phase is switched an additional 180° to model the construction of log-periodic antennas in general. The signal output calculated at the end of the transmission line equation then serves as the output used in computing the antenna response, the second of the three modeling problems.

Modeling Antenna Response

Modeling the performance of the antenna across its bandwidth is a fairly straightforward procedure. For the computation, I employed the NEC computer code³ to calculate the input impedance and transfer function of the antenna due to an incident plane wave at 2-MHz intervals from 2 to 98 MHz (a total of 49 calculations in each instance). The input

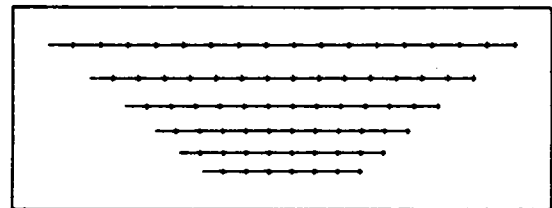


Fig. 2. Computer graphic model of antenna segments.

impedance is found by applying a I - V source signal to the antenna input terminals and then computing the impedance from the resulting current into the antenna. Similarly, the transfer function is found by applying an incident electric field of 1 V/m and then solving for the signal at the input terminals.

Modeling Transient Response

Once the voltage transfer function is known, the response of the antenna to an arbitrary waveform may be found for both the frequency and time domains. The time-domain transient response is found by convolution of the antenna impulse response with the temporal field expression,

$$e_o(t) = \int_0^t h(t - \tau) e_{inc}(\tau) d\tau, \quad (1)$$

where $e_o(t)$ = antenna output voltage, $e_{inc}(t)$ = incident electric field, and $h(t)$ = antenna impulse response in the time domain.

An alternate method of determining the transient response is to perform the convolution first in the

frequency domain—by multiplying the antenna transfer function by the 2- to 98-MHz spectrum of the incident field—and then to perform a Fourier transform to convert the frequency domain to the time domain:

$$E_o(t) = E_{inc}(f) * H(f) \quad (2)$$

and

$$e_o(t) = F^{-1} [E_o(f)] , \quad (3)$$

where F^{-1} is the inverse Fourier operator (Filon's method⁴ is used for the inverse Fourier transform).

RESULTS

In general, the model appears to provide a fairly accurate simulation of the behavior of the log-periodic antenna.

Input Impedance

The input impedance calculated from the model is shown in Figs. 3a and 3b. The real part of the input impedance shown in Fig. 3a varies in the region of 50 Ω over the 30- to 76-MHz frequency design range of the antenna. Similarly, the reactive component of the input impedance is centered on 0 Ω for the same frequency range. The maximum standing-wave ratio for the antenna would be approximately 2.6.

Transfer Functions

Transfer functions for incident plane waves from both the forward and backward directions were computed for the AS-2169/G. Figure 4 shows the calculated gain of the log-periodic array for the forward (boresight) direction falling closely within the antenna's 30- to 76-MHz frequency range. The calculated response appears to agree very well with the experimental continuous-wave test results, another indication of the reliability of the model.

Figure 5 shows the transfer function for an incident wave striking the antenna from the backward direction. Again, the match with experimental data appears close.

Transient Response

To demonstrate the utility of the model in yielding reliable transient response values, I used the experimental data from the measurement of the incident field at the location of the antenna (Fig. 6). The incident field includes the reflected field from the finite ground. (The antenna was removed when the measurements were taken.)

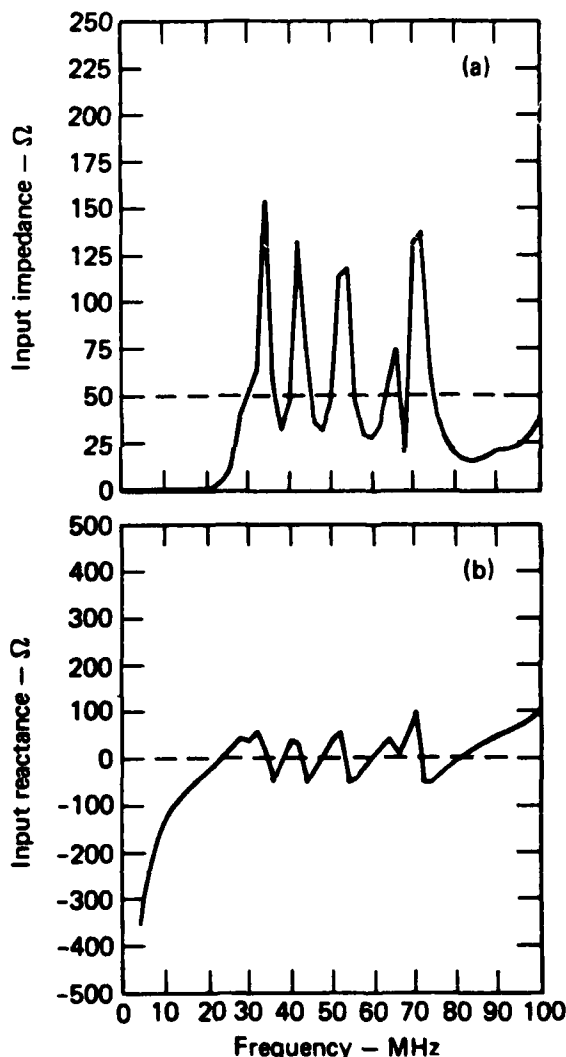


Fig. 3. Calculated input impedance (a) and input reactance (b) of AS-2169/G antenna.

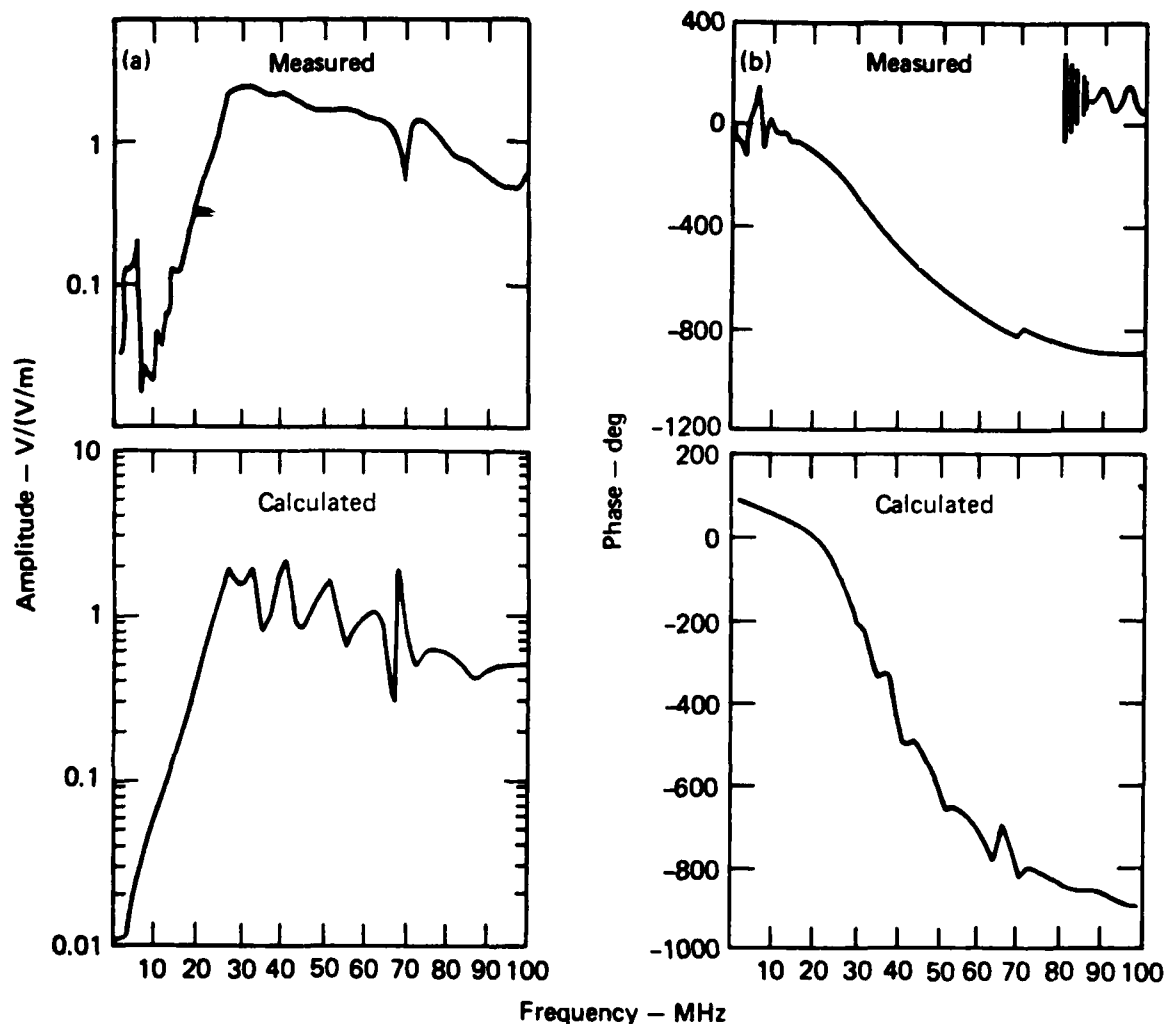


Fig. 4. Calculated and measured voltage transfer functions into a 50- Ω load showing magnitude (a) and phase (b) for forward direction of incident field.

I used Eqs. (2) and (3) to transform the time domain incident field of Fig. 6 to the frequency domain for each of the 49 frequencies of the computed transfer function. The frequency domain equivalent of the incident field was then multiplied by the antenna transfer function to obtain the antenna response in the frequency domain. Finally,

the frequency response was transformed back to the time domain. The results are shown in Figs. 7 (for measured and computed boresight incidence) and 8 (for measured and computed backside incidence). In both instances, there is remarkably good agreement between measurement and computation.

A PRACTICAL EXAMPLE: EMP TRANSIENT RESPONSE

A recurring concern for designers of wide-band antennas that are used under military field conditions is the effect of nuclear electromagnetic pulse (EMP) on communications. The impracticality of

physically simulating EMP conditions suggests the model may have immediate usefulness. The example that follows illustrates this.

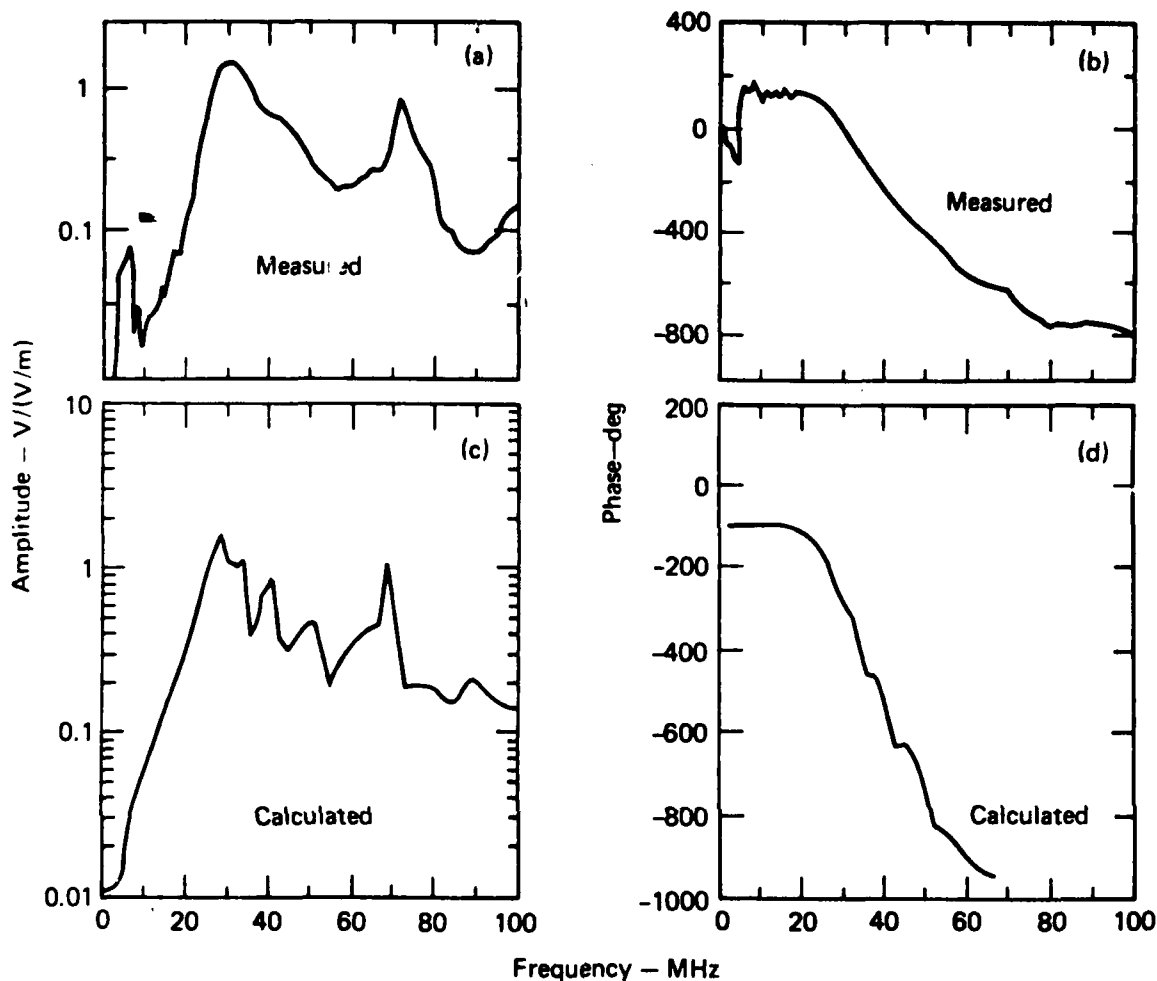


Fig. 5. Computed and measured voltage transfer functions into a 50-Ω load showing magnitude (a) and phase (b) for backward direction of incident field.

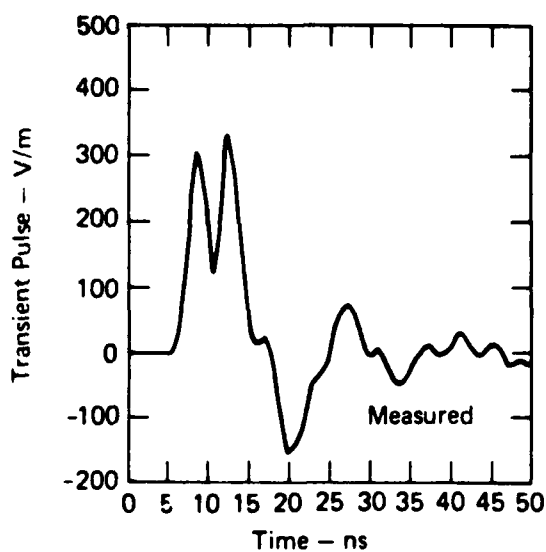


Fig. 6. Experimentally measured incident field at log-periodic antenna.

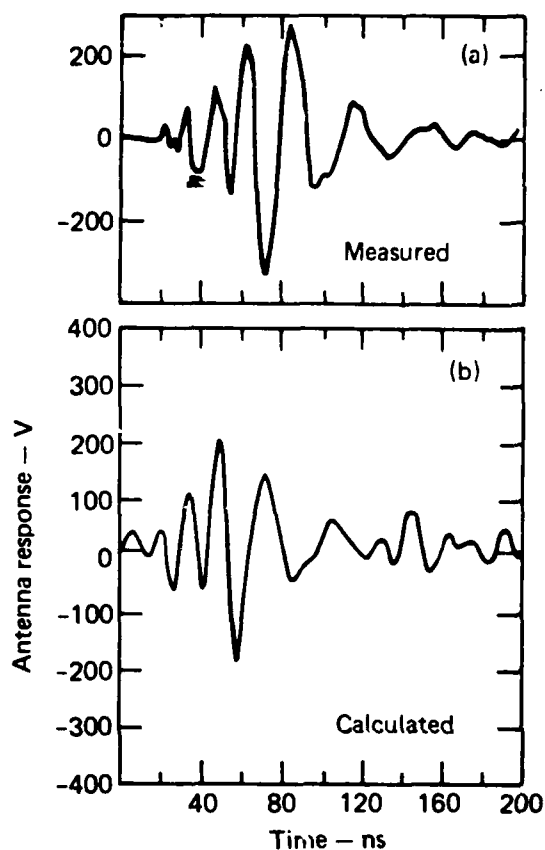


Fig. 7. Calculated and measured transient response of the antenna connected to a 50-Ω load for the incident field of Fig. 6, forward direction.

We begin with a two-term expression that is frequently used for a model of the EMP electric field,

$$e_{EMP}(t) = E_0(e^{-\alpha t} - e^{-\beta t}), \quad (4)$$

where

$$\alpha = 4.0 \times 10^6 \text{ sec}^{-1},$$

$$\beta = 4.76 \times 10^8 \text{ sec}^{-1},$$

and

$$E_0 = 1.05 \text{ V/m}.$$

In the frequency domain the EMP waveform may be written as

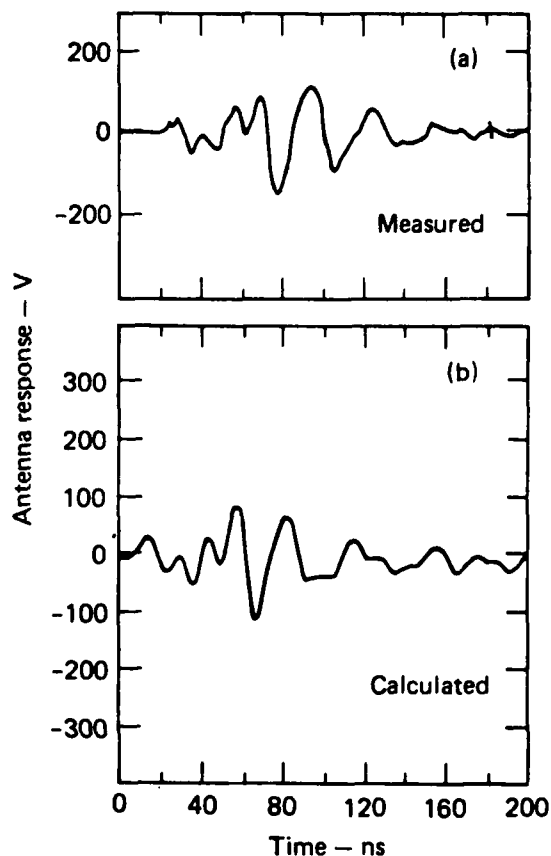


Fig. 8. Calculated and measured transient response of the antenna connected to a 50-Ω load for the incident field of Fig. 6, backward direction.

$$E_{EMP}(s) = E_0 \left(\frac{1}{s + \alpha} - \frac{1}{s + \beta} \right),$$

where

$$s = j\omega. \quad (5)$$

When the antenna is located over a ground plane, we must include both the incident wave and a specular reflected wave from the ground. For a perfect ground, the total field for an EMP wave upon the antenna is

$$E_{TOTAL} = E_{INC} + E_{REFL} \quad (6)$$

$$= E_{EMP} [1 - u(t - \Delta T)] \quad (7)$$

where $u(t - \Delta T) = 0$ for $t < \Delta T$, and ΔT = time delay between the arrival of the incident wave and the reflected wave for an object a distance h above the ground. The delay ΔT is found to be

$$\Delta T = \frac{h}{C \sin \theta_i} (1 - \cos 2\theta_i) , \quad (8)$$

where h = height of the antenna above ground, C = velocity of light, and θ_i = angle of incidence with respect to the ground.

In the frequency domain, the incident EMP wave for the log-periodic antenna over a ground is thus expressed as

$$E(f) = E_{EMP}(f) (1 - e^{-j2\pi\Delta T f}) . \quad (9)$$

If a perfectly conducting ground is assumed, the incident horizontally-polarized electric field undergoes a 180° phase reversal when it reflects from the ground. This reflected field turns off the incident pulse as shown in Fig. 9.

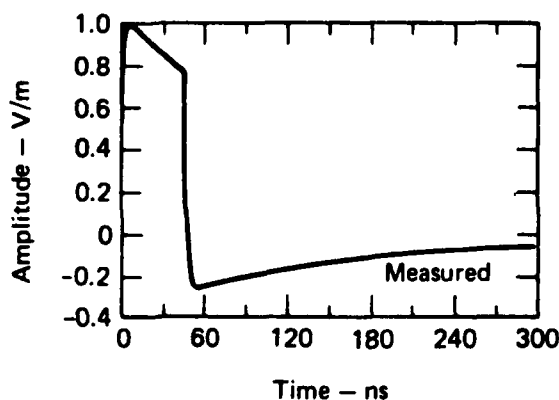


Fig. 9. Total electromagnetic pulse after ground interaction.

Figure 10 shows the results of a two-step procedure: a convolution of the EMP wave with the calculated antenna transfer function followed by a Fourier transform of the results to the time domain. Comparison with the transient response determined from the measured continuous-wave data shows the agreement between the two techniques to be quite good.

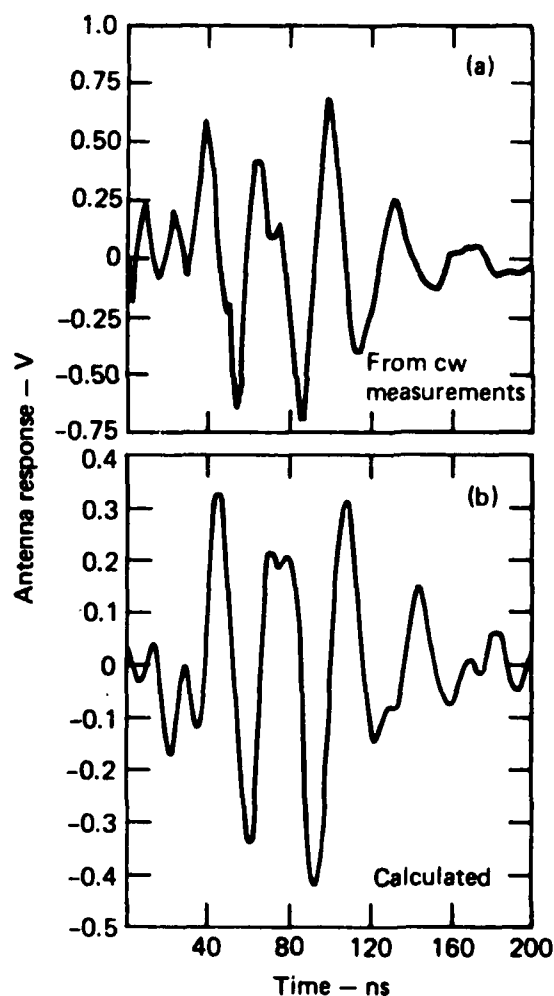


Fig. 10. Calculated EMP response for antenna 10 m above ground plane, compared with response derived from cw measurements.

CONCLUSIONS

In general, the model of the log-periodic antenna provides good agreement with experimental measurements for those aspects of antenna behavior that were examined for this report. Once credibility in the model is established, trade-off studies can be

conveniently made in such areas as angle of incident field, height above ground, etc., to further evaluate the performance of the antenna at very low additional cost.

ACKNOWLEDGMENTS

Particular thanks are due to Werner Stark of the Harry Diamond Laboratories for his help in providing the measured data used for this report and to George Baker of the Defense Nuclear Agency for his helpful comments and suggestions.

REFERENCES

1. Werner J. Stark, *Transient Response of a Log-Periodic Antenna Based on Broad-Band Continuous Wave Measurements*, Harry Diamond Laboratories, Rept. HDL-TR-1792 (April 1977).
2. E. K. Miller, A. J. Poggio, G. J. Burke, and E. S. Selden, "Analysis of Wire Antennas in the Presence of a Conducting Half-Space," *Can. J. Phys.* **50**, 2614 (1972).
3. G. J. Burke and A. J. Poggio, "Numerical Electromagnetics Code (NEC) Method of Moments," Naval Electronics Systems Command, Rept. NOSC/TD116 (July 1977).
4. D. G. Dudley, "Numerical Inversion of the Fourier Transform: A Combination Trapezoidal and Filon Technique," Lawrence Livermore Laboratory, Rept. UCRL-51878 (August 1975).

JRS



MISSION of Rome Air Development Center

RADC plans and executes research, development, test and selected acquisition programs in support of Command, Control Communications and Intelligence (C³I) activities. Technical and engineering support within areas of technical competence is provided to ESD Program Offices (POs) and other ESD elements. The principal technical mission areas are communications, electromagnetic guidance and control, surveillance of ground and aerospace objects, intelligence data collection and handling, information system technology, ionospheric propagation, solid state sciences, microwave physics and electronic reliability, maintainability and compatibility.